Available online at www.sciencedirect.com

ScienceDirect

Underground Space 23 (2025) 193–219

www.keaipublishing.com/undsp

Research Paper

Hygrothermal behavior of energy diaphragm wall and the induced heat and moisture interaction with adjacent underground space

Xu Zhou [a], Xiaoling Cao [a,*], Ziyu Leng [a], Chao Zeng [a], Yanping Yuan [a], Shady Attia [b]

[a] School of Mechanical Engineering, Southwest Jiaotong University, Chengdu 610031, China
[b] Laboratory of Building Materials, University of Liège, Liège 4000, Belgium

Received 13 June 2023; received in revised form 21 January 2025; accepted 23 January 2025
Available online 23 April 2025

Abstract

In the field of design and application of the energy diaphragm wall (EDW), plenty of research was focused on thermal performances and induced mechanical behaviors. The coupled heat and moisture transfer process and the induced impact on the adjacent underground space were lack of attention, which is inevitable due to the high humidity of the surroundings. Therefore, in this paper, a numerical model taking the gradient of the temperature and relative humidity as the driving potential was established to investigate the characteristics of the coupled heat and moisture transfer in the EDW. Firstly, the behavior of the coupled heat and moisture transfer in the summer and winter was investigated separately, and it was compared with the pure thermal model. Results show that the colder the wall surface, the more humid it is. The heat flux is enlarged by the operation of the EDW. Moreover, the heat flux will be underestimated by more than 3.43% in the heat extraction season and by more than 3.90% in the heat injection case if the moisture transfer is not considered. The following long-running investigations have revealed that the latent flux reaches its maximum and minimum value in transition seasons, with a value that is ten times smaller than that of the sensible heat flux. The sensible heat flux reaches 18.7 W/m^2 in summer, while in winter it is −27.4 W/m^2. The peak latent heat flux is reduced by 14.7% as a result of the combined effect of changes in surface temperature and humidity, due to the operation of the EDW. Additionally, the magnitude of these fluxes is affected by the indoor conditions (temperature and relative humidity of the indoor air) and the operating temperature of EDW. Therefore, an orthogonal test is performed to evaluate how much the discrepancies are induced by variations in those parameters. The impact of each parameter varies across the seasons (summer, transition season, and winter). However, the indoor relative humidity has a more significant influence on the water vapor flux in all the seasons. This paper provided details about the coupled heat and moisture transfer process in the EDW. Moreover, it attempts to raise an issue about the impact on the hygrothermal load induced by the heat and moisture flux through the wall surface when applying EDW in underground engineering.

Keywords: Energy diaphragm wall; Coupled heat and moisture transfer; Sensible and latent heat flux; Hygrothermal conditions

1 Introduction

Ground source heat pumps (GHSP) are widely employed in residential spaces to meet the energy consumption of cooling and heating demand, which is an environment-friendly and energy-efficient system (Cao et al., 2015; Yuan et al., 2012). The energy diaphragm wall (EDW) is a type of heat exchanger of the GHSP, which is a special system with a heat exchanger embedded in the underground diaphragm wall such as the basement, underground car parks, metro stations, and shallow light rail tunnels. The fluid circulates in the pipe branches to realize heat absorption or release (Sterpi et al., 2020).

* Corresponding author.
E-mail address: xlcao@swjtu.edu.cn (X. Cao).
Peer review under the responsibility of Tongji University

https://doi.org/10.1016/j.undsp.2025.01.006

In the past twenty years, plenty of research has been oriented toward the thermal, geotechnical, and structural behavior of EDW, by experimental and numerical approaches. Early studies mainly made efforts to unravel the distinct characteristics among the EDW and other energy geostructures, such as the energy piles and tunnels (Adam & Markiewicz, 2009; Brandl, 2006, 2013; Laloui et al., 2006). However, most of the existing research focused on the assessments of thermal performance and influencing factors. Xia et al. (2012) made a first attempt to evaluate the thermal performance of the EDW based on a field experiment at the Shanghai Museum of Nature History. They pointed out that the W-shaped pipe configuration can achieve a heat exchange rate of 40.3, 66.3, and 85.0 W/m at the inlet temperature of 32, 35, and 38 °C, respectively. Moreover, by parametric numerical analyses of the pipe layouts, Sterpi et al. (2014) and Barla et al. (2020) found that the horizontal arrangement with appropriate spacing outperformed the vertical layout in terms of the heat exchange rate. Makasis and Narsilio (2020) conducted an investigation focused on the pipe configurations (i.e., vertically and horizontally designed) and their spacing within the wall. The results showed that there were no thermal profits while varying the total pipe length (by adjusting the pipe spacing) below approximately 300 mm pipe spacing. Additionally, the affecting factors, such as boundary conditions, hydro-geological conditions, concrete thermal properties, and running parameters were intensively investigated (Di Donna et al., 2017, 2021; Makasis et al., 2018, 2020; Zeng et al., 2021).

Apart from the thermal performance, the thermal-induced mechanical behavior of the EDW was another hot spot. Most studies concentrated on the deformation of the wall with the thermal load. The thermally induced mechanical effects were not negligible, and they affected the serviceability of the structure (Habert & Burlon, 2015; Di Donna et al., 2017). Xia et al. (2014) explored the thermal-induced mechanical behavior of the EDW by analyzing the characteristics of heat transfer and the induced thermal stress on the wall cross-section. Bourne-Webb et al. (2016) investigated the thermal–mechanical response of EDW with a seasonal fluctuation temperature condition. Rui and Yin (2018) investigated the wall-soil interaction behavior by conducting a thermo-hydro-mechanical (THM) finite element analysis. They concluded that the seasonal GSHP cycle induced the variation in bending moment on the wall mainly due to the thermal differential across the wall during the winter. Sailer et al. (2019) stated that the behavior of EDW was highly transient, owing to the high rates of heat transfer and pore water pressure dissipation under plane strain assumptions. Dai and Li (2019) established a THM finite element model based on an in-situ EDW at Dean Street Station, UK. Long-term thermal–mechanical performance was discussed considering the ground consolidation, external thermal solicitations, and seasonal geothermal operation. Moreover, a scaled experiment for analyzing the variations in stresses and strains at the wall-soil contact surface was designed by Dong et al. (2019). Li et al. (2020) pointed out that the temperature difference inside the wall was the main reason for the induced thermal stress by a centrifugal experiment.

However, as part of the interior wall of underground buildings which contact with indoor air, the heat release/extraction in the diaphragm wall is non-negligible to the heat and moisture transfer inside and on the surface, which affects the hygrothermal conditions and heat/humidity load (Guimarães et al., 2015; Wang et al., 2018).

The coupled heat and moisture transfer of the envelopes belongs to the field of heat and mass transfer in porous media, and its theoretical research has a long history. A mathematical model of coupled heat and moisture transfer in porous media was originally proposed by Luikov (Luikov, 1964, 1975; Luikov et al., 1968), taking temperature and humidity capacity as the driving potential, the total pressure, concentration gradient, humidity gradient, molecular migration, and capillary action were considered as the affecting factors. Based on the previous works, Colinart et al. (2016) studied the coupled heat and moisture transfer in a coated hemp concrete wall by developing a one-dimensional (1D) model. They emphasized the impact on the water vapor dispersal through the wall surface induced by the weather load (sun, UV, rainfall, etc.). Liu and Huang (2018) analyzed the temperature, relative humidity, and heat flux through the internal surfaces of the expanded polystyrene (EPS) external insulation wall and concrete wall.

Moisture transfer can cause higher latent heat transfer through the envelopes, which has an impact on basement energy consumption. Liu et al. (2015) studied the load through the exterior walls in Chengdu located in a hot-humid area. They pointed out that ignoring moisture transfer will cause a significant discrepancy in predicting the conduction loads. Fang et al. (2020) conducted a dynamic simulation of the hygrothermal behavior concerning external insulation walls and concluded that moisture accumulation risk is great at the interface between insulation and mortar. Xu et al. (2019) investigated the effect of heat and moisture transfer in internal and external wall insulation configurations. They revealed that indoor relative humidity significantly affects the heat transfer process. Wang et al. (2021a) performed a multidimensional analysis of the heat and moisture transfer at the roof-wall corner in high-temperature and high-humidity areas. The influenced zone of the thermal bridge increases by 52.4%, and the overall thermal transmittance of the building node increases by about 55%–77% when considering the moisture transfer through the envelopes. Moon et al. (2014) investigated the impact of moisture transfer on energy efficiency in residential buildings and concluded that the heating load increased by 4.63% and the cooling load increased by 11.26%.

The EDW can be utilized as a part of the basement envelope, where the moisture transfer process is common

due to the high moisture content of the surroundings. However, no studies have been oriented toward the coupled heat and moisture transfer in EDW. The seasonal heat load modes within the heat exchanger embedded in the EDW shall induce a periodic variation of the heat and moisture flux through the surface. The relevant research field lacks attention and the impact on the hygrothermal conditions of the adjacent underground space is uncertain. In this paper, a one-dimensional model was established by the finite difference method (FDM), and performed in the MATLAB software. Usually, the moisture transfer process occurs between the surroundings and indoor air in the horizontal direction. Consequently, a 1D model is an effective tool for predicting the hygrothermal behavior of building envelopes. Temperature and relative humidity gradient were adopted as the driving potentials. Firstly, the behavior of coupled heat and moisture transfer in typical cases (heat injection in summer and heat extraction in winter) was investigated, and they were compared with the results of the pure thermal process. The variation of temperature and relative humidity in the envelopes was analyzed. The impact on the surface hygrothermal conditions and the induced heat and moisture flux through the surface were investigated. Moreover, aiming to reflect the actual long-time operation situations of the EDW, an investigation on seasonal heating–cooling cycles was performed. The surface temperature and relative humidity changes were presented annually. The induced moisture flux, latent and sensible heat flux were discussed separately. In addition, an orthogonal test is performed to evaluate the impact on the sensible heat flux and moisture flux induced by variations in the input parameters, including the operating temperature of EDW and the indoor relative humidity.

2 Model of coupled heat and moisture transfer

2.1 Physical model of the EDW

The profile of the EDW with an adjacent basement is depicted in Fig. 1. Concrete structures integrated with a heat exchanger within the diaphragm wall are the main components, and they are surrounded by soil. In this paper, the coupled heat and moisture transfer and the effects on the hygrothermal conditions of the inner surface are the focus of attention. Therefore, only the portion above the slab is considered. There are four layers of construction. The one exposed to the indoor air is cement mortar, which is 0.01 m in thickness. EPS is implemented as the insulation material, which connects the layers of concrete and mortar. The EPS is 0.05 m in thickness, the concrete layer is 0.6 m, and the soil layer is 1 m (Zeng et al., 2021). The heat exchanger is located in the center of the concrete layer (diaphragm wall domain).

The heat exchanger embedded in the diaphragm wall is a form of heat source, which extracts or injects heat. The detailed heat transfer process and the boundaries are depicted in Fig. 2. The temperature and relative humidity on the right side of the surrounding soil are constant, which is related to the local geological conditions. The wall surface exposed to the indoor air is a heat convection boundary condition. The moisture flow occurred together with the heat flow. The moisture might be transferred from the surroundings to the indoor air under natural conditions due to greater moisture content in the surrounding soil. However, the heat exchanger will induce a temperature rise or drop corresponding to the heat injection or extraction seasons, and it affects the magnitude of the moisture transfer. The driven potentials (relative humidity gradient and temperature gradient) are fully coupled.

The coupled heat and moisture transfer process is a complex issue in porous materials, which will affect the hygrothermal properties of the materials (Wang et al., 2021b). The one-dimensional physical and mathematical model was established. The following assumptions are proposed for the present research before establishing the mathematical model, aiming to simplify the calculation and improve the computational efficiency.

(1) The EDW was applied in the subsurface shelter where air conditioning is necessary. Hence, the indoor hygrothermal conditions are controlled to be a constant value in typical seasons (summer and winter), regarding the suitability of personnel.

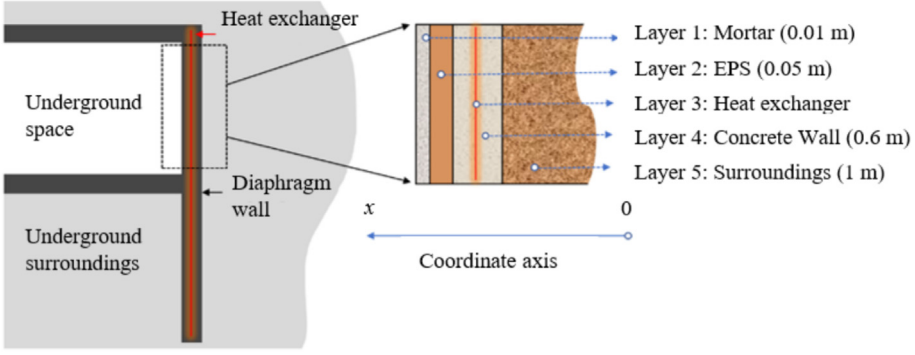

Fig. 1. Schematic of the EDW and the dimensions of each layer in the selection plan.

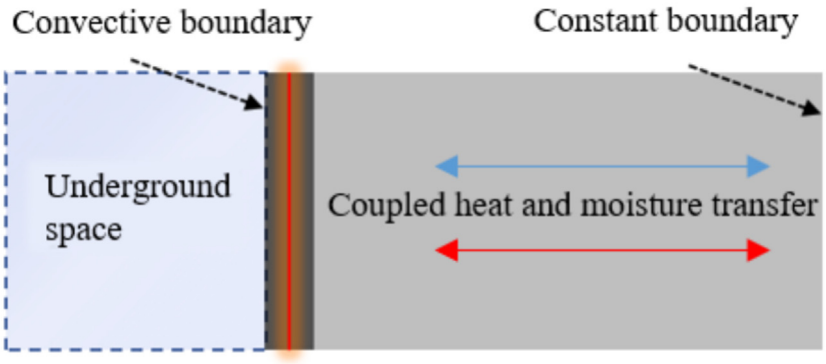

Fig. 2. Schematic of the coupled heat and moisture transfer process.

(2) As the EDW was deep-buried, the influence of meteorological parameters on the soil domain did not exist.
(3) The temperature of the fluid in the heat exchanger is considered constant in summer and winter, and it changes in a ramp trend in transition seasons.
(4) The humid air in the pores satisfies the equation of the ideal gas state and there are two phases of the moisture transfer process, i.e., liquid and vapor.
(5) There is a thermal equilibrium and moisture equilibrium at any location of the envelope materials.
(6) At the interface of the layers, the thermal and moisture contact resistance is not considered.

2.2 Mathematical model of coupled heat and moisture transfer

2.2.1 Moisture transfer

There are two phases of water vapor and liquid transferred in the porous building materials. As described by Eq. (1) (Wang et al., 2021b):

$$\frac{\partial w}{\partial t} = -\nabla(g_v + g_l), \tag{1}$$

where w is the moisture content (kg/m^3); g_v and g_l represent the water vapor flux and the liquid flux (kg/(m^2•s)), respectively.

Equation (1) is expanded into the form of related material properties parameter as Eq. (2) (Liu et al., 2015; Wang et al., 2021b):

$$\xi\frac{\partial\phi}{\partial t} = \frac{\partial}{\partial x}\left(\delta_v p_{v,sat}\frac{\partial\phi}{\partial x} + \delta_v\phi\frac{\partial p_{v,sat}}{\partial T}\frac{\partial T}{\partial x}\right) + \frac{\partial}{\partial x}\left(K_l\rho_l R_v \times \frac{T+273.15}{\phi}\frac{\partial\phi}{\partial x} + K_l\rho_l R_v \ln(\phi)\frac{\partial T}{\partial x}\right), \tag{2}$$

where $\xi = \frac{\partial w}{\partial \phi}$ represents the sorption capacity of the specific material; δ_v denotes the water vapor permeability (kg/(Pa•m•s)); $p_{v,sat}$ is the partial pressure of saturated water vapor (Pa), which can be derived from Eq. (3) (Branco et al., 2004); T is the temperature (°C); ϕ denotes the relative humidity (%); K_l is the permeability of the liquid water (kg/(Pa•m•s)), which can be calculated by Eq. (4) (Wang et al., 2021a); R_v is the gas constant of water vapor, which is 462 J/(kg•K); ρ_l is the density of the liquid water (kg/m^3); D_v is the water vapor diffusivity (m^2/s); $\rho_{v,sat}$ is the saturated water vapor density (kg/m^3).

$$p_{v,sat}(T) = 610.5\,e^{\left(\frac{17.269T}{237.3+T}\right)}, \tag{3}$$

$$K_l = \frac{D_v\phi\rho_{v,sat}}{R_v T\rho_l}. \tag{4}$$

Then the governing equation for the moisture transfer process can be reduced to Eq. (5). The coefficients D_ϕ and D_T are expressed as a function of relative humidity and temperature, as shown in Eqs. (6) and (7), respectively.

$$\xi\frac{\partial\phi}{\partial t} = \frac{\partial}{\partial x}\left(D_\phi\frac{\partial\phi}{\partial x} + D_T\frac{\partial T}{\partial x}\right), \tag{5}$$

$$D_\phi = \delta_v p_{v,sat} + K_l\rho_l R_v\frac{T+273.15}{\phi}, \tag{6}$$

$$D_T = \delta_v\phi\frac{\partial p_{v,sat}}{\partial T} + K_l\rho_l R_v\ln(\phi). \tag{7}$$

2.2.2 Heat transfer

The water vapor condenses in the pores due to capillary action, resulting in a phase change process within the materials and acting as a heat source or sink. By this characteristic, moisture transfer and heat transfer are coupled. Hence The process of heat transfer is mainly divided into two parts: conduction and convection. The energy conservation equation can be expressed as the following Eq. (8) (Wang et al., 2018):

$$\frac{\partial E}{\partial t} = -\nabla(q_{cond} + q_{conv}) + q_{sour}, \tag{8}$$

where q_{cond} and q_{conv} represent the energy transferred by conduction and convective (W/m^2), respectively; q_{sour} denotes the inner heat source, which is generally neglected

in conventional conditions. However, the heat source exists within the EDW.

Equation (8) is expanded into the form of related material properties parameters as Eq. (9) (Wang et al., 2021b):

$$(\rho_m c_m + w c_l)\frac{\partial T}{\partial t} = \nabla\left[L\delta_v p_{v,sat}\nabla\phi + \left(\lambda_w + L\delta_v\phi\frac{\partial p_{v,sat}}{\partial T}\right)\nabla T\right] + q_{sour}, \quad (9)$$

where λ_w is the thermal conductivity (W/(m•K)); c_l indicates the specific heat capacity of the liquid water (J/(kg•K)); ρ_m denotes the density of the dry material (kg/m^3); c_m indicates the specific heat capacity of the dry material (J/(kg•K)); L is the latent heat of vaporization of water vapor, which is equal to enthalpy difference between water vapor and liquid water, and represented as a function of temperature shown in Eq. (10) (Zhou et al., 2002):

$$L = (2500 - 2.4T)\times 10^3. \quad (10)$$

The coefficients A_ϕ and A_T, are introduced to describe the governing equation concisely, as shown in Eqs. (11)–(13). A_T can be regarded as the equivalent thermal conductivity under the impact of moisture transfer.

$$(\rho_m c_m + w c_l)\frac{\partial T}{\partial t} = \nabla\left[A_\phi\nabla\phi + A_T\nabla T\right] + q_{sour}, \quad (11)$$

$$A_\phi = L(T)\delta_v p_{v,sat}, \quad (12)$$

$$A_T = \lambda_w + L(T)\delta_v\phi\frac{\partial p_{v,sat}}{\partial T}. \quad (13)$$

2.2.3 Boundary conditions

The boundaries at the wall surface exposed to the indoor air are convective mass and heat transfer between the surface and the air. The heat flux consists of the sensible heat of heat convection and the latent heat of vaporization and condensation. The mass flux is dependent on differences in the relative humidity and the saturated vapor pressure between the surface and indoor air. The value of the undisturbed boundaries at the soil side remains unchanged in the temporal dimension. Moreover, the relative humidity of indoor air is set at a comfortable level (ϕ = 50%), while the temperature of indoor air varies with the seasons.

The boundaries of the moisture transfer process are as follows (Wang et al., 2018, 2021a, 2021b):

$$\begin{cases} \phi_{soil}(0,t) = \phi_{cons} \\ \phi_{indoor}(t) = \phi_{cons} \\ g = \beta_i(\phi_{indoor}p_{sat,indoor} - \phi_{sur}p_{sat,sur}) \end{cases}, \quad (14)$$

where t denotes the time (s); ϕ_{cons} is a constant value of relative humidity applied to the boundary; g is the local mass flux through the wall surface (kg/(m^2•s)); β_i is the coefficient of the mass transfer (kg/(m^2•s•Pa)); the subscripts sat and sur represent the saturation and surface, respectively.

The boundaries of the heat transfer process are as follows:

$$\begin{cases} T_{soil}(0,t) = T_{cons} \\ T_{indoor}(t) = T(t) \\ q = h_i(T_{indoor} - T_i) + \beta_i L(\phi_{indoor}p_{sat,indoor} - \phi_{sur}p_{sat,sur}) \end{cases}, \quad (15)$$

where the T_{cons} is a constant value of temperature applied to the boundary; q is the local heat flux through the wall surface (W/m^2); h_i is the coefficient of the convective heat transfer of the wall surface.

In this investigation, the coefficient of the convective heat transfer is 8.7 W/(m^2•K), which is suggested in the national standard of China (Ministry of Housing and Urban-Rural Development of the People's Republic of China, 2016). The coefficient of the mass transfer β_i is related to h_i, which can be obtained from the Lewis analogy (Liu et al., 2015) as Eq. (16):

$$\beta_i = 7.7\times 10^{-9}h_i. \quad (16)$$

The heat exchanger embedded in the diaphragm wall is a heat source, which generates or absorbs energy into or from the surroundings. As shown in Fig. 3, a virtual node is introduced to represent the heat exchanger, and it is supposed to be installed in the middle of the two adjacent nodes. Therefore, the term q_{sour} of Eq. (8) should be considered when describing the energy conservation equation for these two adjacent nodes, while it is omitted for the other nodes. It is obtained as the following Eq. (17):

$$q_{sour} = A_T\nabla\left(\frac{(T_f - T_{i(i+1)})}{\frac{\Delta x}{2}}\right), \quad (17)$$

where T_f denotes the temperature of the fluid (°C), and Δx is the size of the grids.

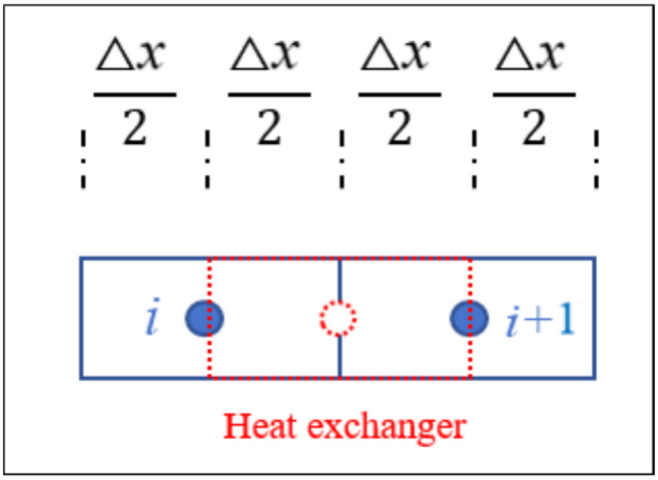

Fig. 3. Schematic of the influence of heat exchanger on the adjacent nodes (i, i+1 are the node numbers).

Table 1
Thermophysical properties of the materials.

Layers	Water vapor permeability kg/(m · s · Pa)	Thermal conductivity W/(m · K)	Specific heat J/(kg · K)	Density kg/m^3	Moisture content kg/m^3
Soil	$\frac{2.13 \times 10^{-6}}{R_v(T+273.15)}$	1.21	920	2400	$38.4\phi^{15.2} + 60\phi^{0.45}$
Concrete	$3.09 \times 10^{-14} + 5.51 \times 10^{-12}\phi^{20.7}$	$1.38 + 0.0032w$	837	2500	$\frac{\phi}{0.018\phi^2 - 0.027\phi + 0.02}$
EPS	1.1×10^{-11}	$0.0331 + 0.001\ 23w$	1470	30	$\frac{\phi}{-0.527\phi^2 + 0.964\phi + 0.0708}$
Mortar	5.467×10^{-11}	$1.965 + 0.0045w$	840	1807	$\frac{\phi}{-0.022\phi^2 + 0.025\phi + 0.0001}$

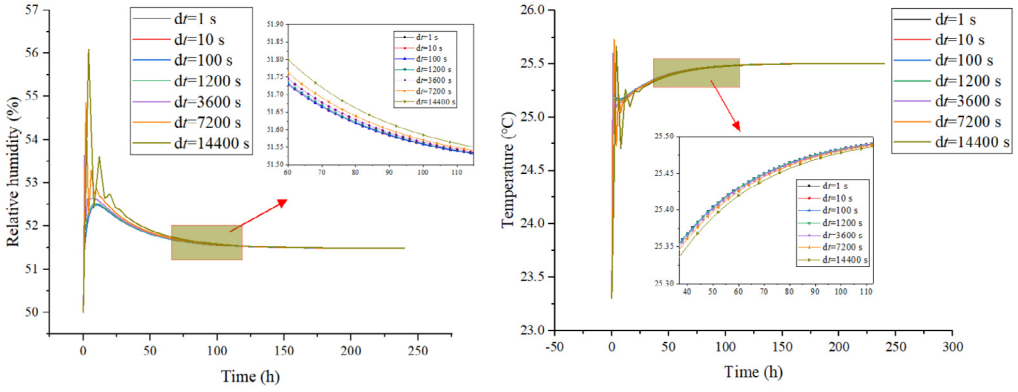

(a) (b)

Fig. 4. Independence tests of the time-step size. (a) Relative humidity, and (b) temperature.

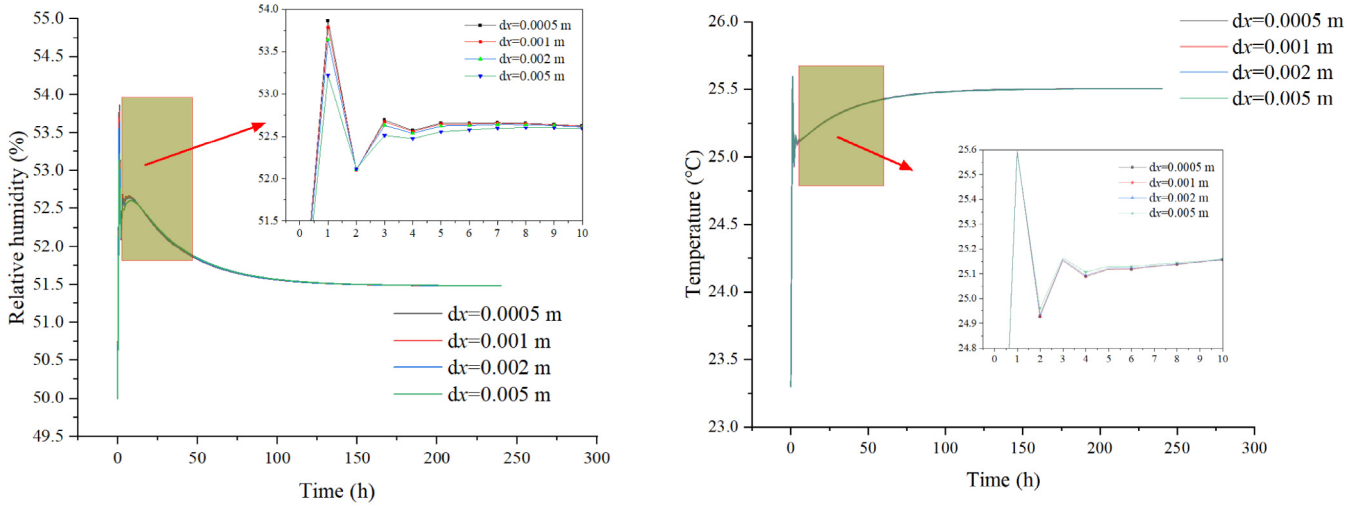

(a) (b)

Fig. 5. Independence tests of the grid size. (a) Relative humidity, and (b) temperature.

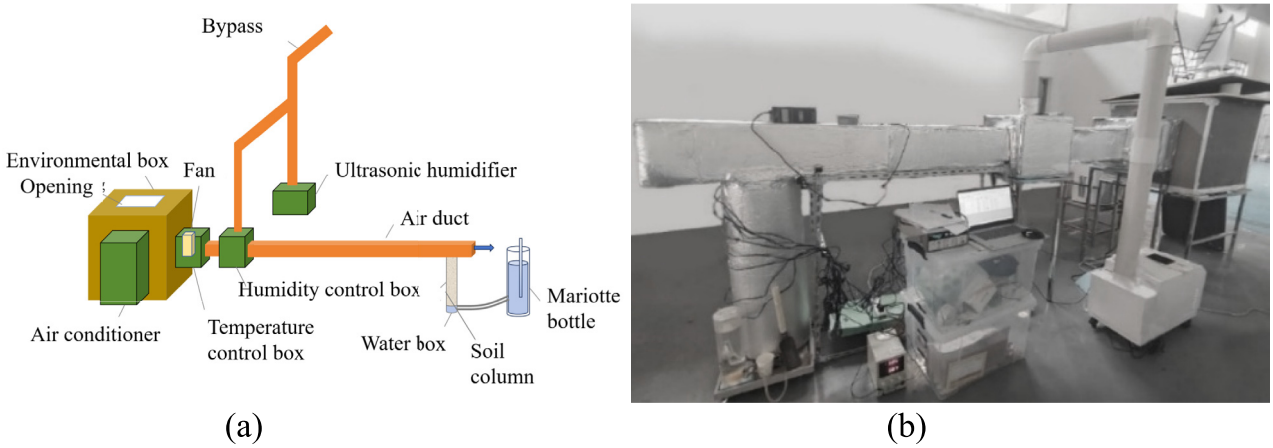

Fig. 6. (a) Schematic diagram, and (b) site photos of the laboratory experiment.

2.3 Numerical solution and verification

2.3.1 Material properties

The detailed thermophysical properties of the materials in different layers are listed in Table 1. The vapor diffusivity of the soil is $D_v = 2.13 \times 10^{-6}$ m$^2 \cdot$ s, which is quoted from the literature of Zanden and Schoenmakers (1996). Moreover, it can be converted to vapor permeability by the formula $\delta_v = \frac{D_v}{R_v(T+273.15)}$ (kg/(m $\cdot$ s $\cdot$ Pa)) (Wang et al., 2021a). The parameters of thermal conductivity, specific heat, and the density of the soil are 1.21 W/(m•K), 920 J/(kg•K), and 2400 kg/m^3, respectively, referred to the research of Wang et al. (2016). Moreover, the moisture content was fitted as a function of relative humidity with the experiment data by Yan (2003), which is expressed as $38.4\phi^{15.2}+60\phi^{0.45}$ $\left(\mathrm{kg/m^3}\right)$. The thermophysical properties of the other building materials are selected from the literature (Kumaran, 1996; Li et al., 2009; Wang et al., 2021b).

2.3.2 Grid and time-step independence analysis

The accuracy and efficiency of the numerical method are related to the time step and the size of the grid, so the independence tests are carried out under various grid sizes and time-step sizes. The results are shown in Figs. 4 and 5. It is obvious that the time-step size has a significant influence on the numerical stability at the initial stage, but the discrepancies among these cases are quite minor after 2 days. Moreover, the grid size causes a negligible impact on the results. Considering that the operation of EDW is long, the dt = 3600 s and dx = 0.002 m are chosen in the following investigation.

2.3.3 Validation with experimental results and the literature works

(1) Validation with a laboratory experiment

A laboratory experiment was conducted to examine the accuracy of the numerical method in predicting the coupled heat and moisture transfer process. The experimental system is shown in Fig. 6, which mainly includes four parts: environment box, air duct, unsaturated soil column, and the mariotte-bottle water supply system. The environment box can provide the airflow of constant temperature and humidity with an air conditioner. This airflow can impose a high-temperature boundary on the surface of the unsaturated soil column. The mariotte bottle can maintain constant temperature and humidity boundary at the bottom boundary of the soil column. The schematic diagram of the conditions is shown in Fig. 7. The density and specific heat capacity of the soil are 1850 kg/m^3 and 1750 J/(kg•K), respectively. The initial temperature and moisture content of the soil column are 16.5 °C and 80 kg/m^3, respectively. At the top of the soil column, the temperature and relative humidity are 25 °C and 60%, respectively. The transfer of heat and moisture within the materials is driven by the tem-

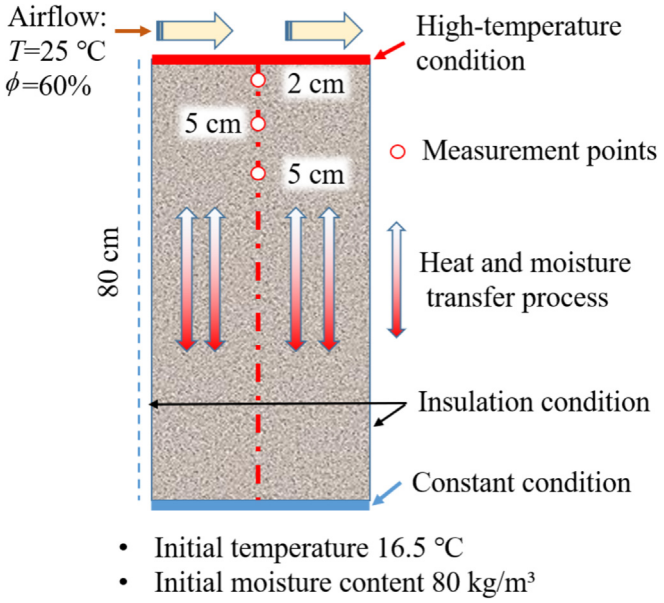

Fig. 7. Schematic diagram of coupled heat and moisture transfer process in the unsaturated soil column.

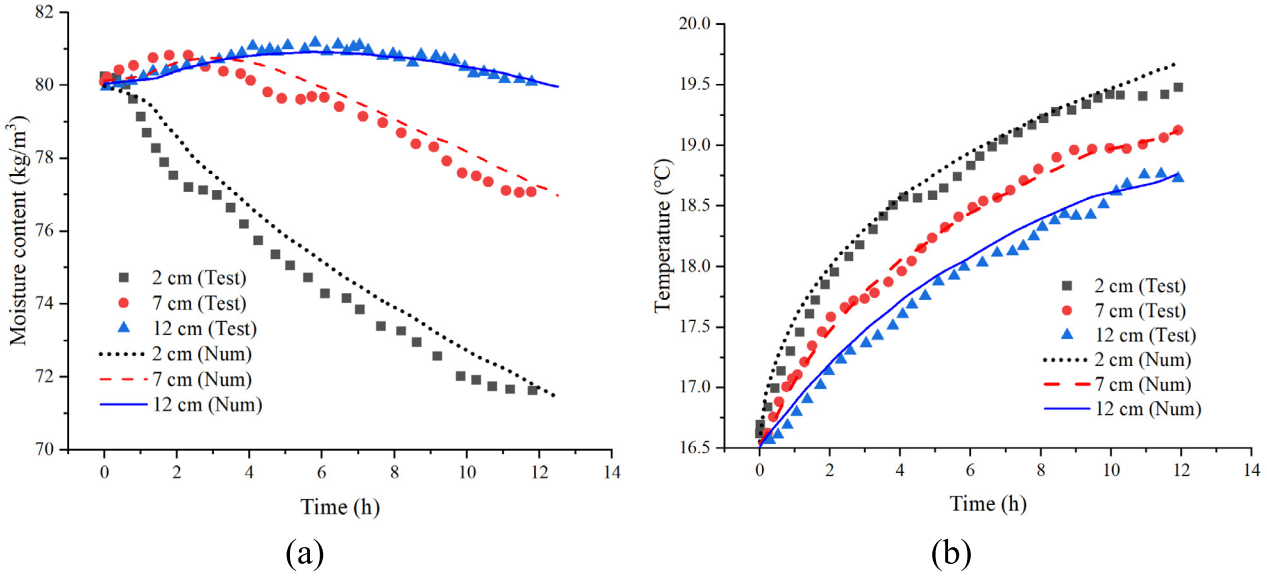

Fig. 8. Comparison between the numerical and experiment results. (a) Variation of moisture content, and (b) temperature at different depth.

perature and humidity gradients. The maximum discrepancies between the numerical results and experiment results are within 3%, which is within the acceptable limits, as depicted in Fig. 8.

(2) Validation with the literature works

To evaluate the accuracy of the numerical results, the model of this paper is also compared with the experiment research published by Steeman et al. (2009). In their

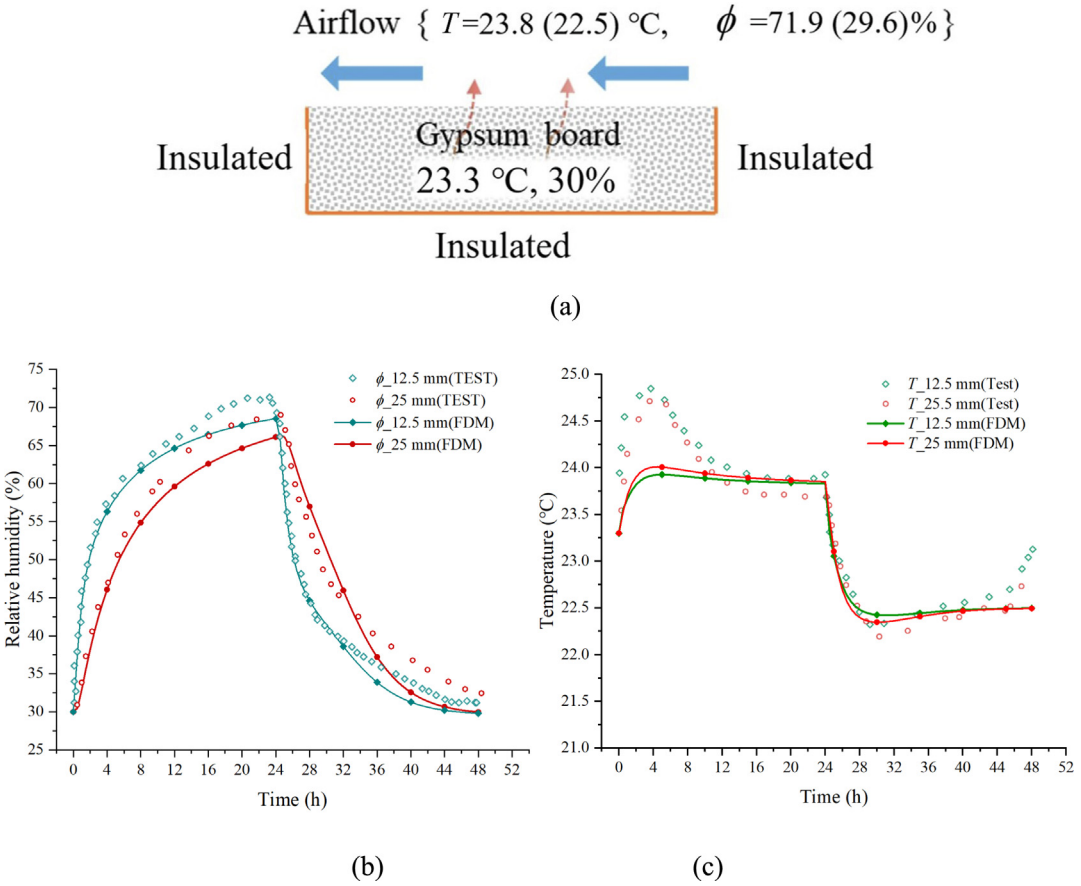

Fig. 9. Validation with the work of Steeman et al. (2009). (a) Model and boundaries, (b) relative humidity, and (c) temperature.

research, high and low levels of temperature and relative humidity boundaries are applied to investigate the response of an uncoated gypsum board in sorption and desorption conditions. The details of the boundaries are shown in Fig. 9(a). The thermal properties of the gypsum board are as follows: the density is 690 kg/m^3, the specific heat is 840 J/(kg•K) and the thermal conductivity is 0.198 W/(m•K). These values are consistent with those reported in the literature. The results of the relative humidity and temperature in a heating–cooling cycle are depicted in Fig. 9(b) and (c). The maximum relative discrepancies of relative humidity between the values of the Test and FDM are no more than 8%. A possible reason is that the function of moisture content is a result of polynomial fitting, and there is an arithmetic error. Moreover, The maximum differences in temperature are within 5%. The maximum differences occurred at the initial stage, which might be due to the weak prediction of the start-up of the experiment. Disturbance can exist when hot and humid airflow over the surface initially, and the thermal and humid state of the airflow is not stable. Hence, the discrepancies are within acceptable limits, and the FDM can be used to calculate the heat and moisture transfer process in this paper.

Also, this model was validated with the British Standard EN 15026 (British Standard Institution, 2007). This benchmark test deals with a semi-infinite homogeneous material in equilibrium with a constant climate, which is widely adopted to validate the numerical model for heat and moisture evolution in building materials. The comparisons between the simulation results and the EN 15026 are added, as shown in Fig. 10, and the results show a good agreement with each other.

3 Results and discussion

The behavior of coupled heat and moisture transfer in EDW varies with different seasonal conditions. The details of the model have been described in Section 2.1. The effects during typical cases (heat injection in summer and extraction in winter) are investigated in Sections 3.1 and 3.2. The impact on the hygrothermal load of the indoor air induced by the long-term thermal cycles (heating–cooling cycles) is analyzed in Section 3.3. Moreover, a sensitivity analysis of the model's parameters is conducted in Section 3.4 to investigate how variations in the input parameters affect the heat and moisture fluxes through the internal surface.

3.1 Heat and moisture transfer in heat injection case

The initial temperatures of the concrete and soil are 12.5 °C, and the initial relative humidity is 85%. Mankibi et al. (2015) analyzed the annual variation of the soil temperature at different depths in Beijing, China. The periodic temperature amplitude is within 2.5 °C at a depth of over 3.2 m. Here, the EDW was assumed to be deep-buried, and the temperature and relative humidity were considered constant to simplify the numerical model. The temperature of the indoor air is 26 °C and the relative humidity is 50%, and they were within the thermal comfort standards (Djongyang et al., 2010). The initial relative humidity of the EPS and mortar layers is 50%, considering the EPS and mortar layers are close to the indoor space. The initial temperature of the EPS and mortar is 12.5 °C. Additionally, the temperature of the heat exchanger is set as 35 °C, which is considered the average temperature of the fluid (Barla et al., 2020).

In the summer case, the heat exchanger embedded in the diaphragm wall is a high-temperature heat source. Figure 11 shows the results of the temperature and relative humidity within the layers after 120 days. The "heat" denotes the heat injection case, "non" represents the case without a heat source (conventional wall), and "heat conductive only" indicates the model of pure thermal process

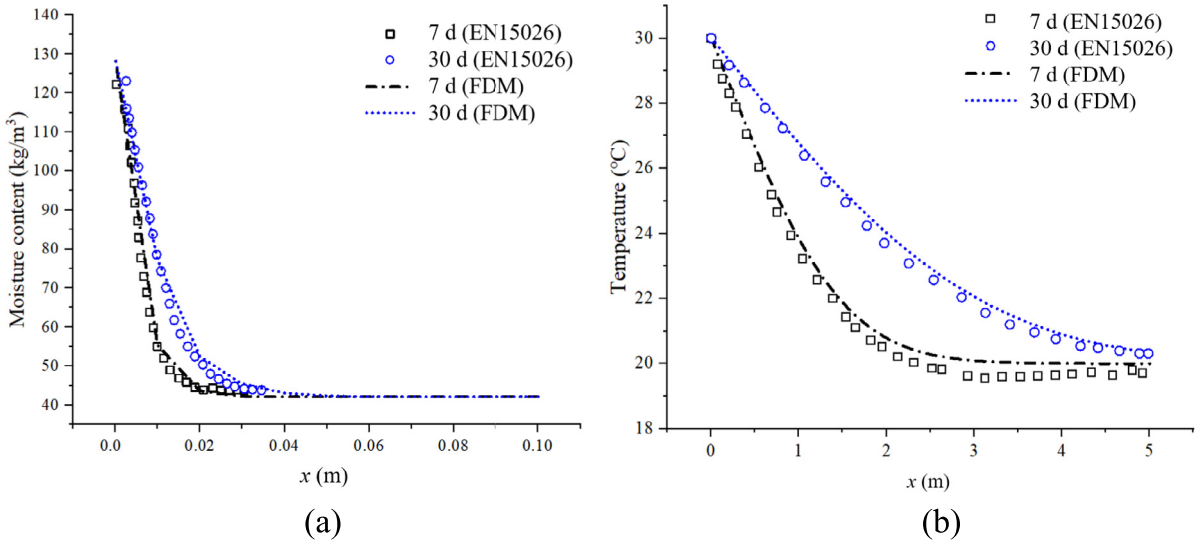

Fig. 10. Comparison with the EN 15026. (a) Variation of moisture content, and (b) temperature at different depth.

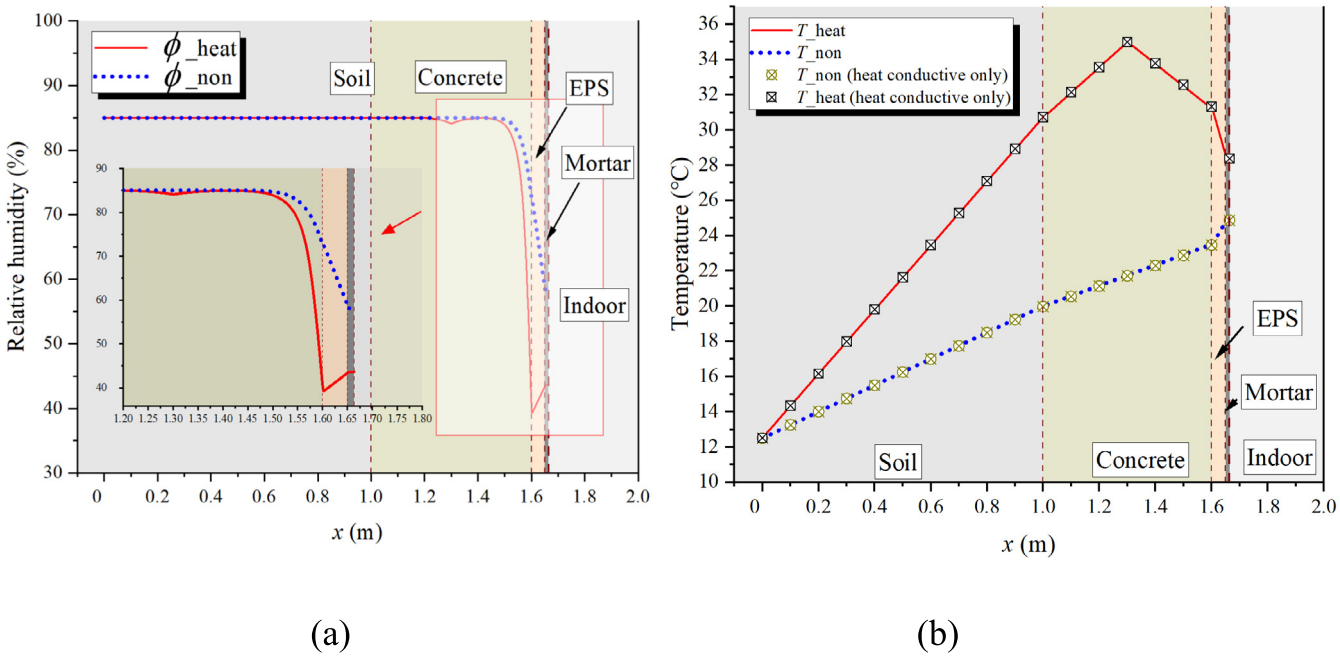

Fig. 11. Distribution of the temperature and relative humidity after 120 days in summer case. (a) Relative humidity, and (b) temperature.

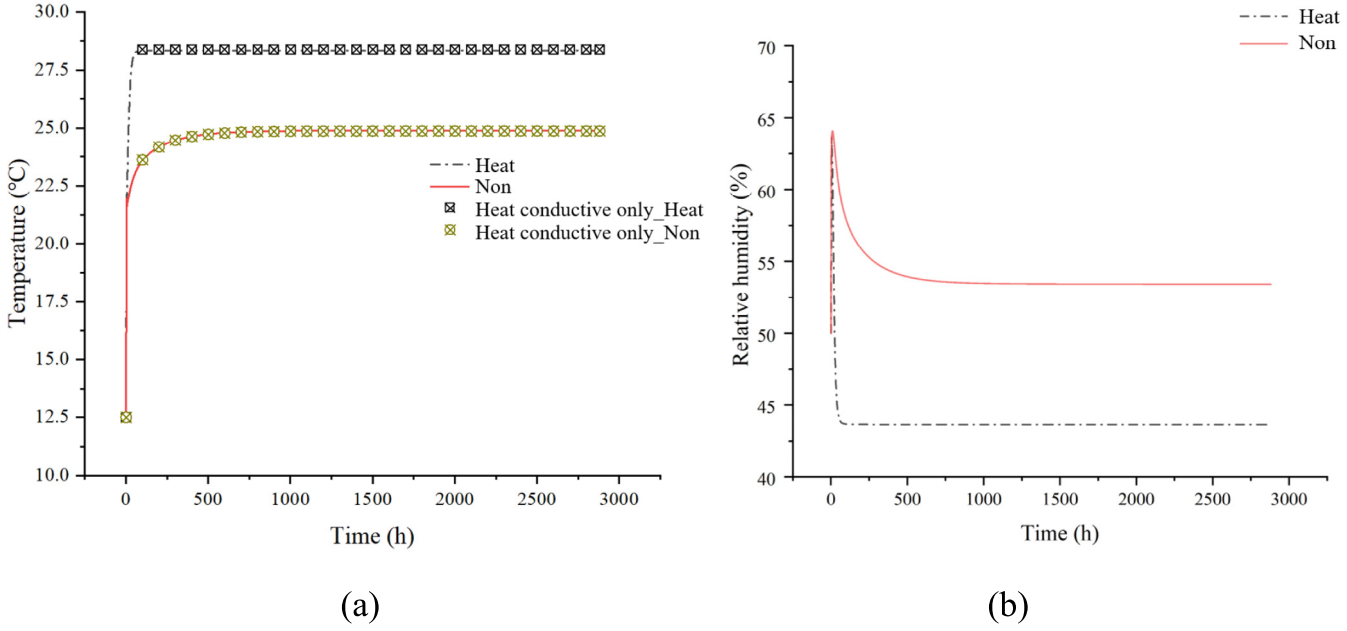

Fig. 12. Temperature and relative humidity at the inner surface in summer case. (a) Temperature, and (b) relative humidity.

(without moisture transfer process). It is obvious that the high-temperature area is located around the heat exchanger, as shown in Fig. 11(b). In the layer of EPS and mortar, the temperature rises due to the heat transfer process. There is a turning point at the interface of the EPS and concrete due to the thermal insulation effect of the EPS. The insulation layer has a very low thermal conductivity, which prevents heat transfer. Moreover, the metope is heated by the operation of the EDW, and the temperature increases to about 24.9 °C after 120 days. Additionally, the results of the pure thermal process show little difference from the other cases. This is due to the relatively minor magnitude of the moisture transfer process and the limited induced temperature variation. However, the impact on the

adjacent underground space needs more discussion, because the moisture permeates into the indoor environment and causes additional latent heat and humidity load. Moreover, the impact on the moisture transfer is depicted in Fig. 11(a). The inner surface shows a 12.7% decrease in relative humidity, which indicates that the moisture in the envelope layers is transmitted into the indoor environment. The temperature gradient between the air and the wall surface is part of the cause of this phenomenon (Eqs. (5) and (11)). The heated wall surface will force the moisture content transferred into the indoor space, which can be conceptualized as a process of heat and drying. Furthermore, the relative humidity in the envelope layers exhibits a disparate variation between the "heat" and "non" cases, which can be attributed to the disparate magnitude of the thermal transfer process. The lower relative humidity in the EPS (compared to that in the concrete and mortar layers) shall be due to the insulation effect (low permeability) and the weak moisture absorption capacity.

The temperature variations of the EDW with elapsed times are depicted in Fig. 12(a). It is obvious that the temperature rise in EDW is much greater than that in the conventional wall. The "heat conductive only" case still shows little difference. Figure 9(b) gives the relative humidity variations of the EDW with elapsed times. All the changes meet the expected effect, that is the more the wall is heated, the hotter and drier (low humidity level) it is. The surface relative humidity rises in the initial stage, while it drops as time prolongs. This is because the initial indoor temperature is higher than the surface temperature, and the moisture content permeates into the envelopes by the driving potential of the temperature difference. With the increase of the surface temperature, the moisture is transferred into the indoor air, and the relative humidity goes down. The turning points at the interface of materials in both temperature and relative humidity are due to the physical properties' differences. The insulation effect of the EPS is apparent, especially in the temperature field.

Temperature and humidity changes will induce the variation of heat and moisture flux through the inner surface, as shown in Fig. 13. The positive value indicates the direction from envelopes to indoor air, while the negative value indicates the opposite direction. The heat flux rises rapidly and reaches a stable status in 100 h in the EDW. The operation of the EDW alters the direction of the heat flux and induces an approximately 18.7 W/m additional thermal load of the underground space. It is worth noting that if the moisture transfer process ("heat conductive only" case) is not considered, the heat flux gain (from the surface to the indoor) will be underestimated by 3.09% ("heat" case), and overvalued by 5.03% ("non" case). The difference is due to latent heat caused by the moisture transfer process, as depicted in Fig. 13(b). The moisture flux in the "heat" case is positive, hence the latent heat flux through the surface interior, and not taking into account moisture transfer will underestimates heat flux. On the contrary, the moisture flux in the "non" case is negative, and the latent flux acts as a heat loss for the indoor environment, hence not taking into account moisture transfer will overvalue the heat flux gain (if we consider it as heat loss, it is still an underestimation).

The distributions of temperature and relative humidity at different elapsed times are depicted in Figs. 14 and 15, respectively. It can be seen that the temperature changes

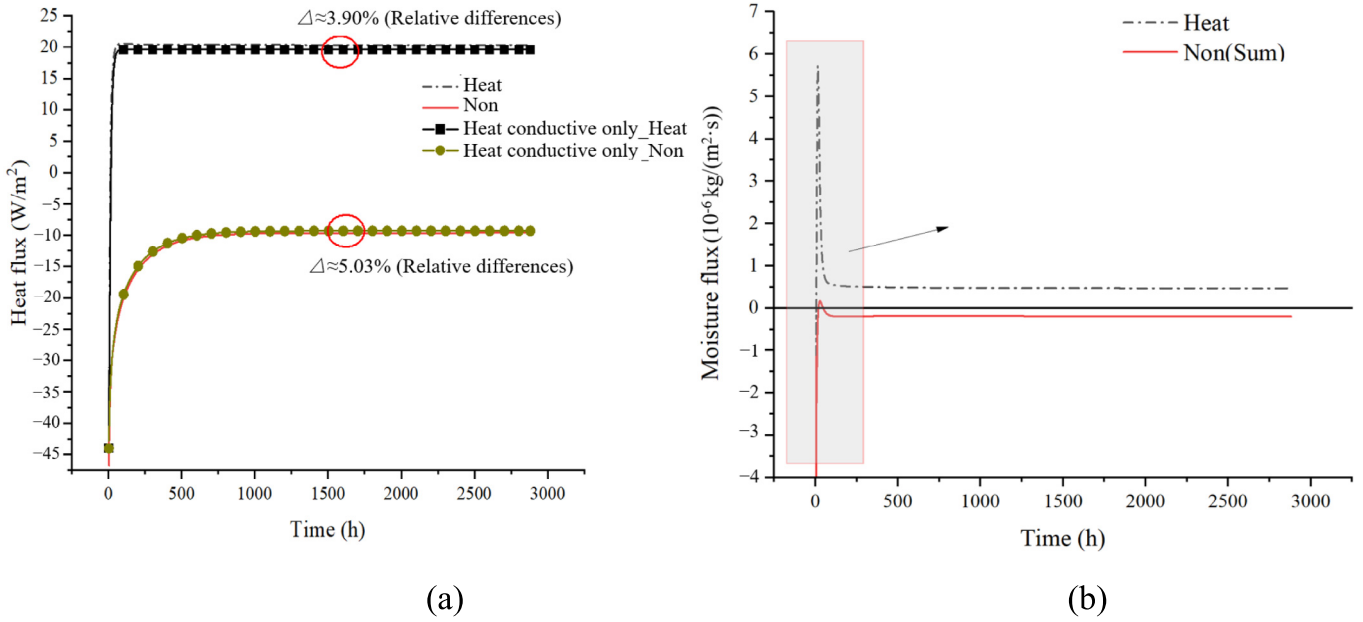

Fig. 13. Variation of the heat and moisture flux through the inner surface in summer case. (a) Heat flux, and (b) moisture flux.

obviously in the early 96 h, and the magnitude in EDW is much greater than that in the conventional wall. Then it reaches a steady state (Fig. 14(b) and (d)). However, the relative humidity changes relatively slowly, the difference in relative humidity between the layers in space is relatively obvious in days. This is because the magnitude of the moisture transfer process is very small, and the cumulative effect on the time dimension is gradually apparent.

3.2 Heat and moisture transfer in the heat extraction case

The initial conditions stay the same as those in the heat injection case. However, the temperature of the heat exchanger in the heat extraction case is considered 5 °C, and the indoor air temperature is 18 °C. The indoor relative humidity is the same as that in the summer case.

As depicted in Fig. 16, an opposite heat and humidity behavior is observed in the winter case. The "cool" denotes the heat extraction case. The thermal insulation effect of the EPS still exists at the interface. A 17.0% decrease in surface temperature is observed compared to that of the pure thermal process, which indicates that the heat loss from envelopes is strengthened. Similar to the summer case, the temperature field without considering the moisture permeation shows a little difference. This is because the temperature change caused by moisture transfer is small.

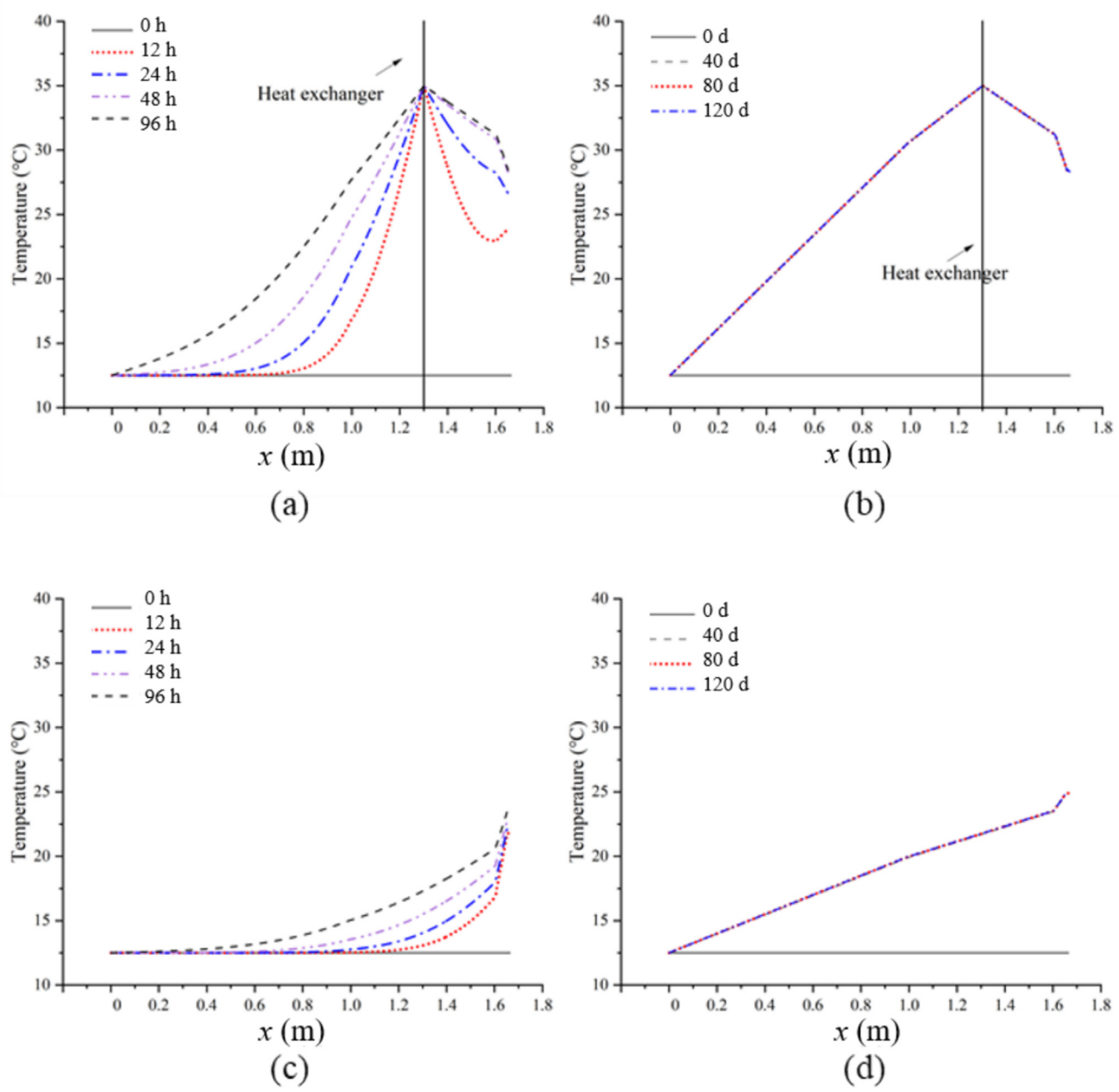

Fig. 14. Distribution of the temperature at different elapsed times in the summer case. (a), (b) EDW, and (c), (d) conventional wall.

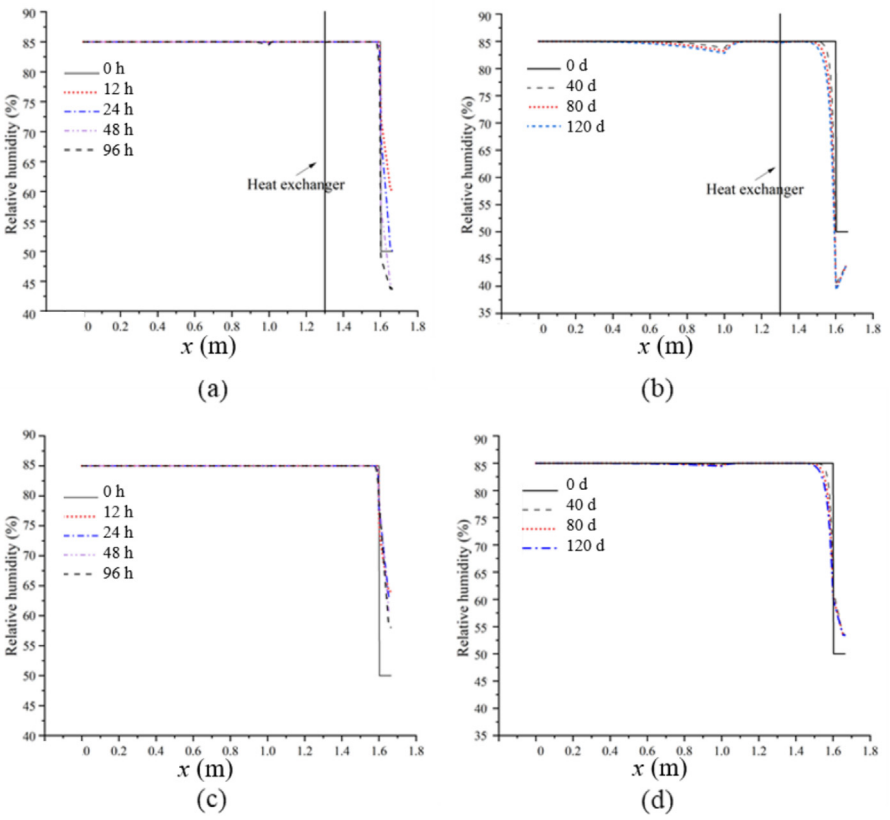

Fig. 15. Distribution of the relative humidity at different elapsed times in the summer case. (a), (b) EDW, and (c), (d) conventional wall.

Additionally, a 21.0% increase in relative humidity at the inner surface is found, which should be due to the cooling effect changes in local saturation conditions. Moreover, this phenomenon can be summarized as the colder the surface, the more humid it is, as shown in Fig. 17. The peak temperature in the "cool" case is induced by indoor air

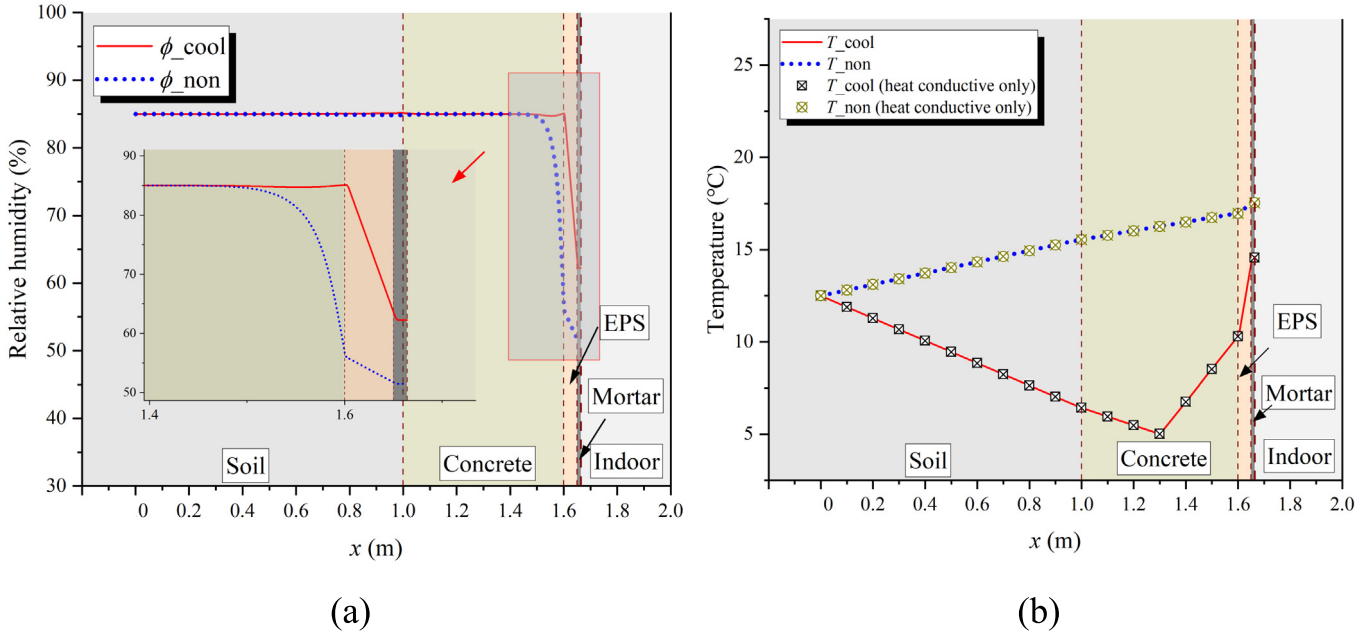

Fig. 16. Distribution of the temperature and relative humidity after 120 days in winter case. (a) Relative humidity, and (b) temperature.

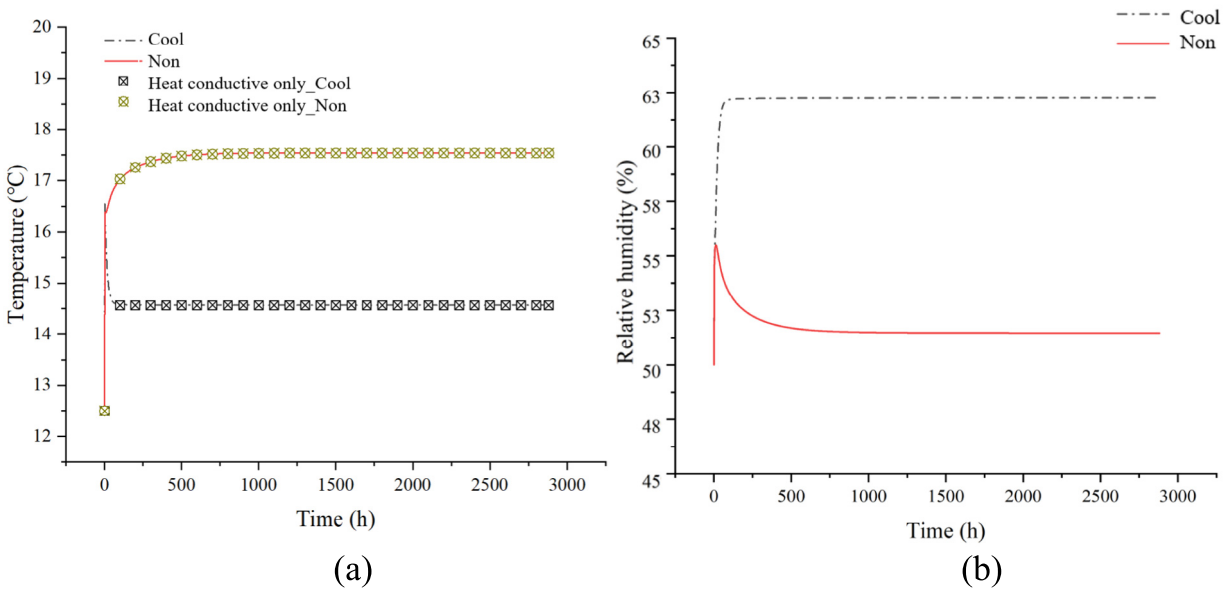

Fig. 17. Temperature and relative humidity at the inner surface in winter case. (a) Temperature, and (b) relative humidity.

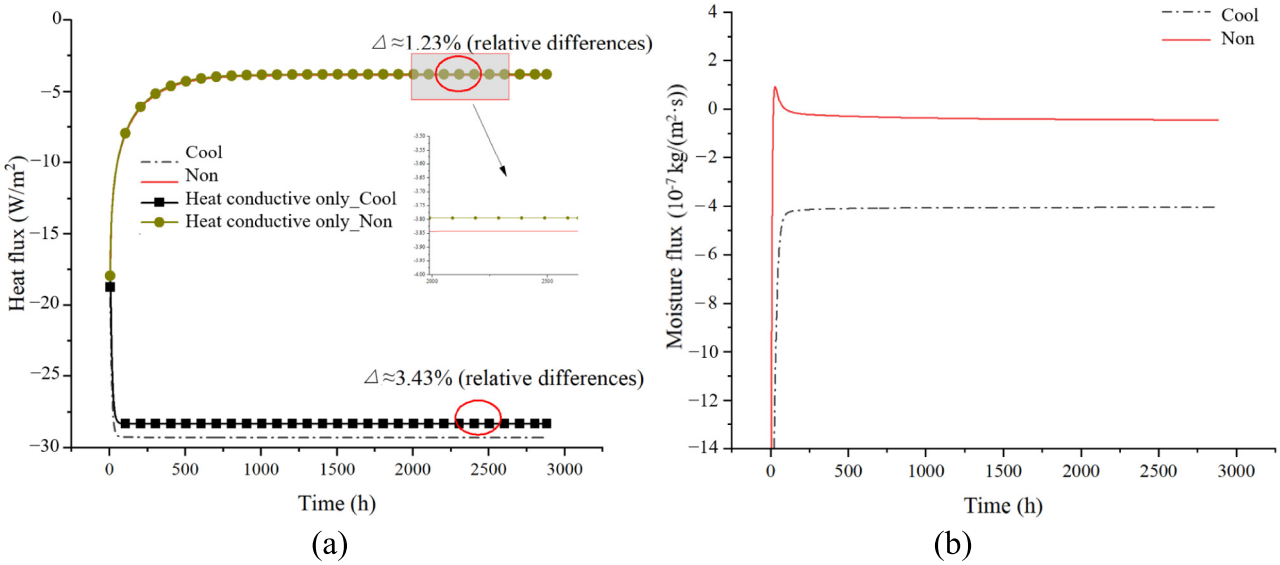

Fig. 18. Variation of the heat and moisture flux through the inner surface in winter case. (a) Heat flux, and (b) moisture flux.

heating. With the time prolonged, the response of the low-temperature heat source reaches the surface and the temperature goes down. Moreover, the relative humidity rises rapidly to approximately 62.3% in the "cool" case, while it shows a drop to about 51.5% in the "non" case. The differences in relative humidity between the surface and indoor air (50%) are due to the driven potential caused by the temperature gradient between them.

The heat and moisture flux in winter show a different trend compared with those in the summer case, as depicted in Fig. 18. The "cool" case shows a greater heat loss from the indoor air to envelopes (negative value) than "non" case, this is a consequence of heat extraction process. It is worth noting that if not taking the moisture transfer into consideration, the heat loss from the surface will be underestimated by 3.43%. This is due to ignoring the latent heat caused by the mass transfer process (Fig. 18(b)).

The temperature of the inner surface reaches approximately 17.6 °C in the "non" case, as shown in Fig. 19(d). However, in the "cool" case, the surface temperature drops to about 14.6 °C. This is because the heat extraction process takes away a lot of heat energy, as shown in Fig. 19 (b). The relative humidity varies with the operating temperature, as depicted in Fig. 20. The envelopes maintain a higher humid condition in the "cool" case, which indicates that the colder the materials the more humid it is. Additionally, there are almost no turning points in the distribu-

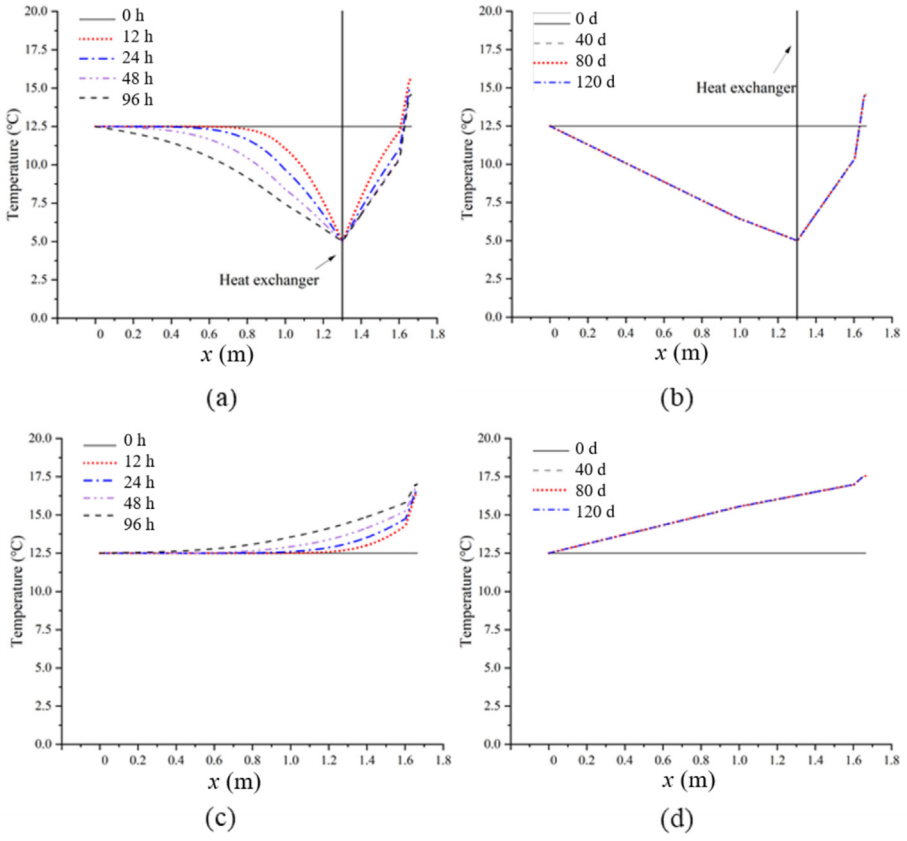

Fig. 19. Distribution of the temperature at different elapsed times in the winter case. (a), (b) EDW, and (c), (d) conventional wall.

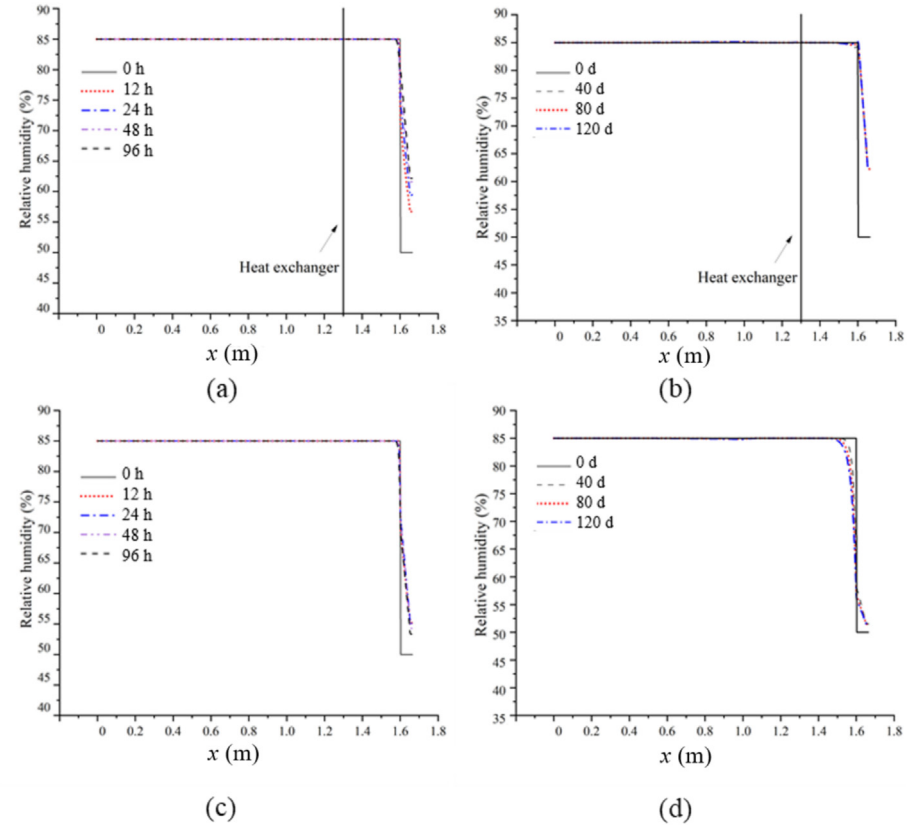

Fig. 20. Distribution of the relative humidity at different elapsed times in the winter case. (a), (b) EDW, and (c), (d) conventional wall.

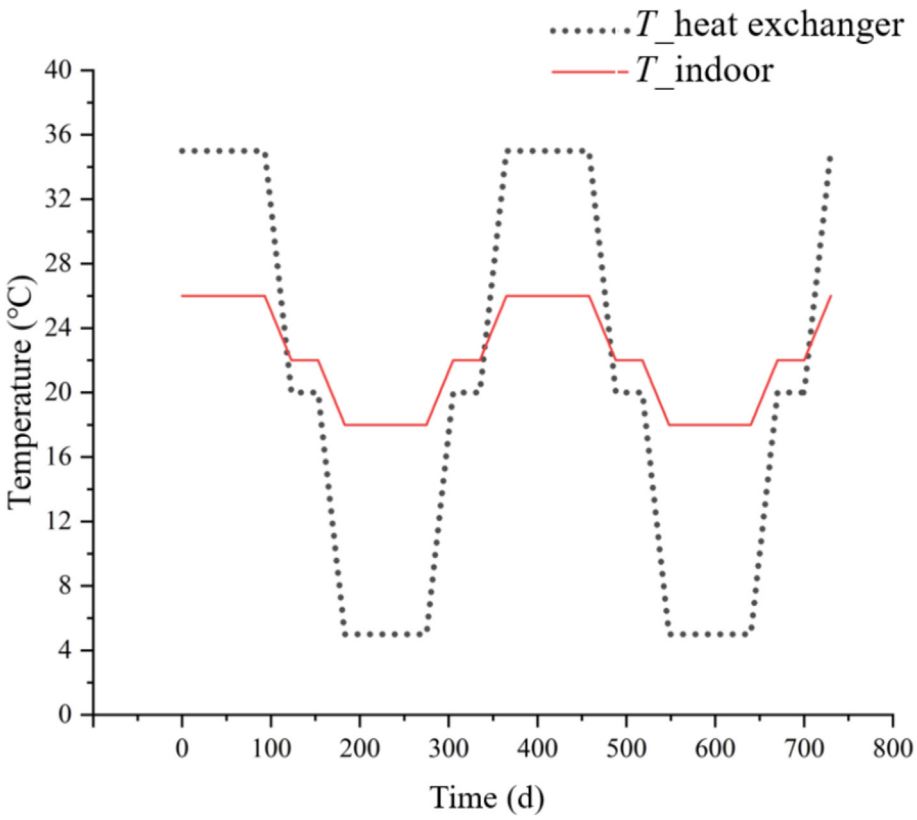

Fig. 21. Temperature of the heat exchanger and indoor air in periodic cycles.

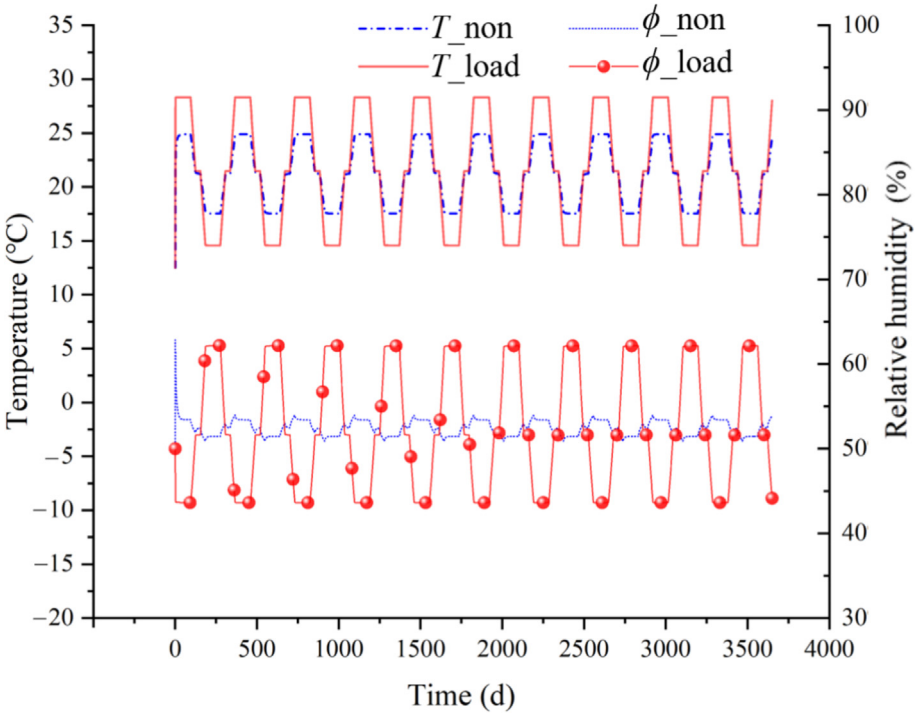

Fig. 22. Temperature and relative humidity at the surface.

tion of the relative humidity caused by the properties' differences in materials. This is because all the materials have a high level of initial moisture content, and the cooling effect induced by the heat extraction causes no moisture loss but gain.

Summarily, both the heat injection and heat extraction of the EDW can lead to an obvious variation in hygrothermal conditions of the inner surface. The insulating layer can block part of the water vapor penetration. Therefore, when applying EDW in underground space, these effects should be considered, which are often ignored in previous studies.

3.3 Heat and moisture transfer in a long-term periodic cycle

The investigations above help us to understand the behavior of the coupled heat and moisture transfer in typical cases, but they can not provide information about the actual long-time operation situations. In this section, attention is mainly paid to the behavior of the coupled heat and moisture transfer in annual heating-cooling cycles.

The initial conditions stay the same as those in the heat injection case. The temperature of the heat exchanger and indoor air changes with the seasons, while the relative humidity of indoor air remains at 50% all the time. As shown in Fig. 21, the temperatures of the heat exchanger and indoor air are 35 and 26 °C in summer, respectively. While in winter, they are 5 and 18 °C, respectively. However, the temperatures of the heat exchanger and indoor air change in a ramp trend in transition seasons. Besides, there is a stable period of 30 days. These considerations were introduced in the literature of Barla et al. (2020). The long-term investigation starts from the beginning of the heat injection season.

The temperature and relative humidity show a periodic variation, as depicted in Fig. 22. The temperature and relative humidity in the case with thermal load ("load" case) are much greater than that in the case without thermal load ("non" case). It is worth noting that the phase of the periodic changing relative humidity in the "load" case differs from that in the "non" case. This is because the material has the ability to store moisture, so there is a hysteresis effect. The relative humidity at the inner surface reaches its maximum level in winter under the "load" case, while it decreases to its minimum level in winter under the "non" case. This is because the heat extraction in winter causes the wall temperature to decrease, and increases the relative humidity. Moreover, the temperature decreases to nearly the same level in both the "load" and "non" cases in transition seasons (135th and 315th d), as shown in Fig. 23. It differs quite a lot in summer and winter due to the significant heat injection and extraction process, respectively. The same phenomenon is found in surface relative humidity, as depicted in Fig. 24. The operation of the EDW can lead to

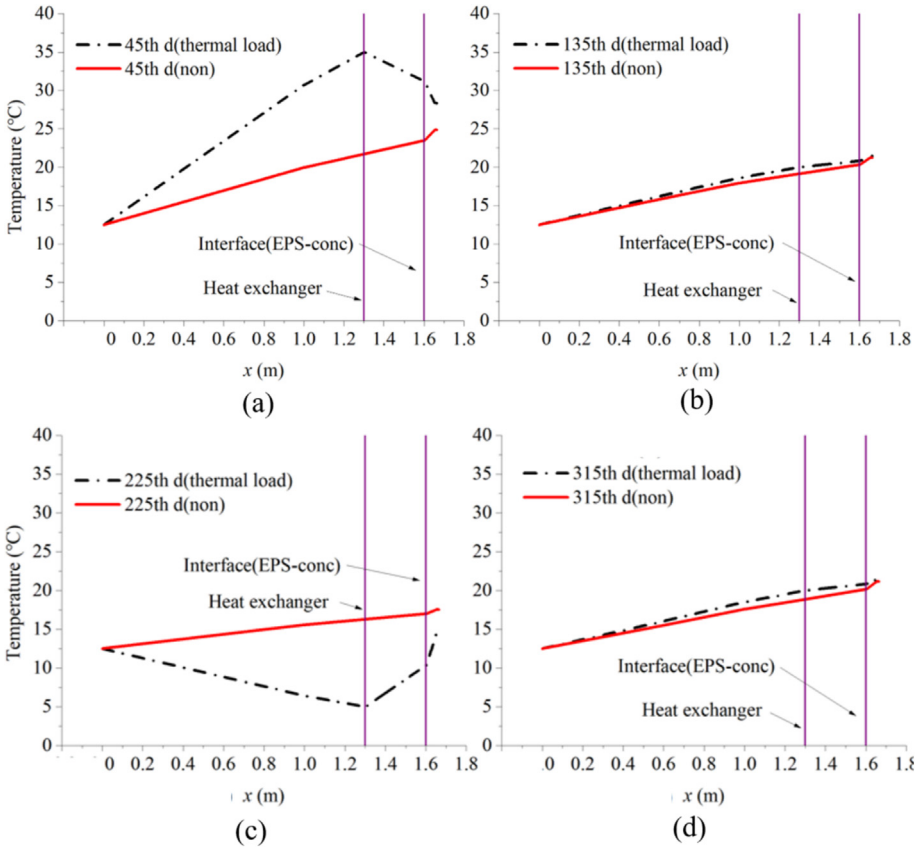

Fig. 23. Distribution of the temperature at different elapsed time. (a) 45th d, (b) 135th d, (c) 225th d, and (d) 315th d.

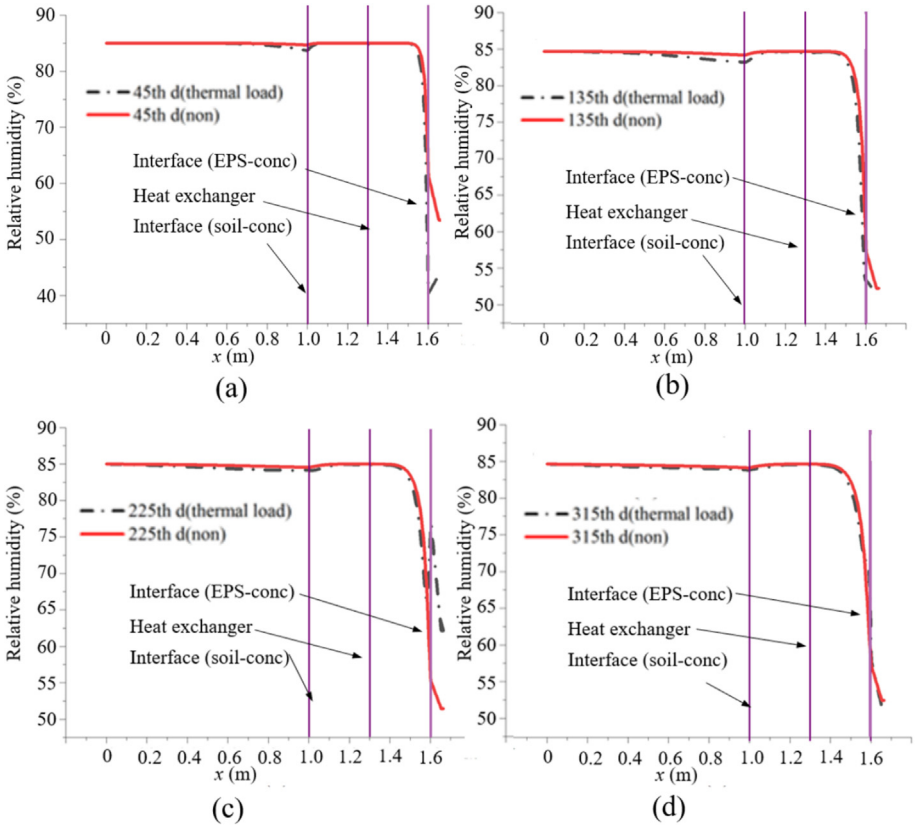

Fig. 24. Distribution of the relative humidity at different elapsed time. (a) 45th d, (b) 135th d, (c) 225th d, and (d) 315th d.

an obvious variation in hygrothermal conditions of the inner surface.

The induced additional heat and moisture flux through the envelopes are shown in Fig. 25(a). The heat flux is partially compensated in a complete cycle, but the moisture flux can be considered fully compensated. This might be due to that the heat transfer process of the material is much greater than the moisture transfer process, resulting in a more obvious change in heat flux. The phase of periodically varied heat flux through the wall surface is half a cycle ahead in the "load" case. This is also because of the hysteresis effect induced by the material's ability to store moisture. Moreover, the maximum moisture flux was restrained by 14.7% comparing that in the "load" case to that in the "non" case. The changes in surface hygrothermal conditions are the primary cause.

As depicted in Fig. 25(b), the sensible heat is affected significantly during the operation period of the EDW. The sensible heat flux is approximately 18.7 and −27.4 W/m^2 in summer and winter, respectively. Moreover, the latent heat is suppressed when there is a thermal load within the EDW. This is probably due to changes in hygrothermal conditions (partial pressure of saturated water vapor and relative humidity), which induce a restricted moisture permeation process.

Interestingly, the peak value of the latent heat occurs in transition seasons, which is along with the greatest moisture flux shown in Fig. 25(a). This is because the latent heat flux depends on the amount of moisture flux. The magnitude of the moisture transfer process is influenced by the relative humidity and partial pressure of saturated water vapor at the current time step, according to Eq. (14). Aiming to reveal the cause of the great moisture transfer process in transition seasons, Fig. 25(c) depicts the relative humidity and partial pressure of saturated water vapor of the wall surface and indoor air. The partial pressure of saturated water vapor reaches its maximum and minimum value during the summer and winter, respectively. However, the relative humidity at the wall surface reaches its minimum and maximum value during the summer and winter, respectively. The product of pressure and relative humidity at the surface is not much distinct from that of the indoor air, in summer and winter. Hence, the moisture flux through the surface is limited. However, in transition seasons, the partial pressure of saturated water vapor decreases. Meanwhile, the relative humidity increases. The product of pressure and relative humidity of the surface follows the change of time, and it becomes distinct from that of indoor air. Consequently, the moisture flux through the inner surface increases and reaches its maximum level. The amount of moisture transfer in transition seasons of the "non" case is more than that of the "load" case, as shown in Fig. 26(b) (data for the second, third, and fourth years

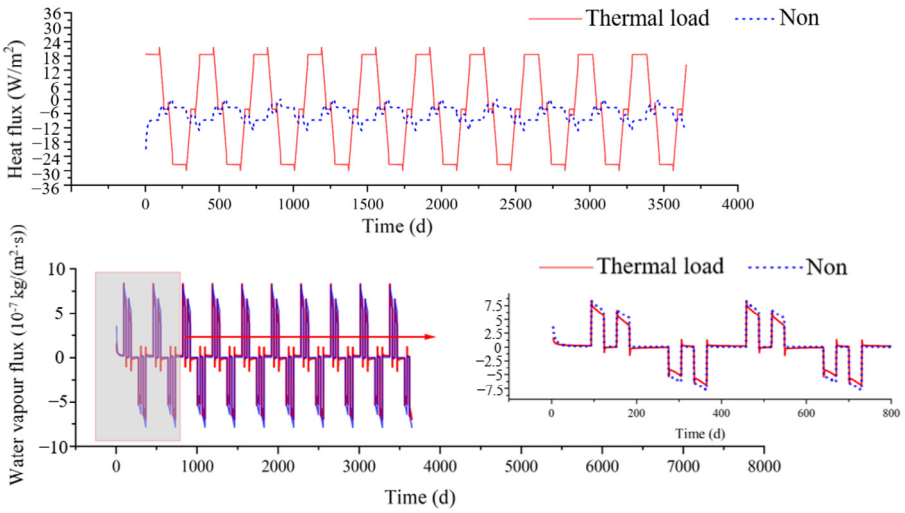

(a)

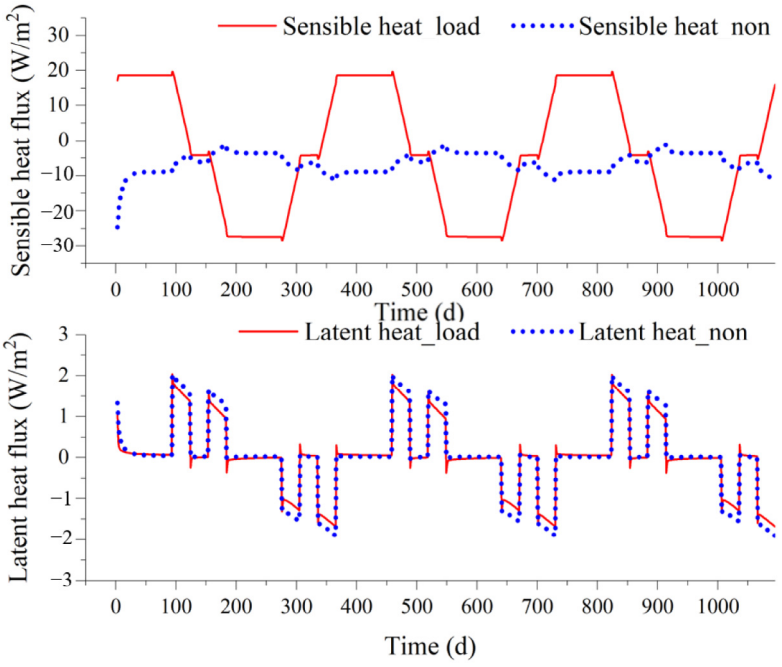

(b)

Fig. 25. Flux of the heat and water vapor. (a) Total flux of heat and water vapor, (b) flux of sensible heat and latent heat, and (c) relative humidity and partial pressure of saturated water vapor.

of this investigation are analyzed to avoid interference from initial conditions in the first year).

The amount of both total heat and sensible heat transfer in the "load" case is significant in summer and winter, as depicted in Fig. 26(a) and (c). However, in transition seasons, the amount of heat transfer in the "non" case is higher than that in the "load" case. Wall temperature variation in transition season affected by the heat source in the "load" case shall be the reason. The more obvious the difference between the wall temperature and the indoor temperature under the influence of EDW, the greater the heat transfer. The latent heat in transition seasons is quite great, which is related to the moisture transfer. The changes of humidity and partial pressure of saturated water vapor on the surface are more complex in the transition seasons (as shown in Fig. 25(c)), which leads to greater moisture transfer.

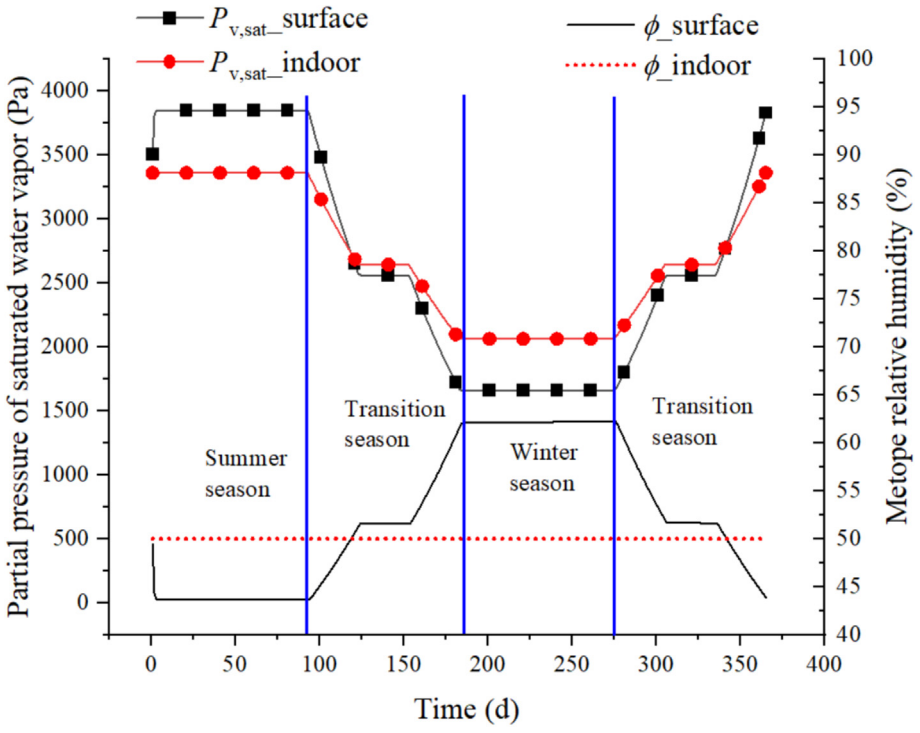

(c)

Fig 25. *(continued)*

3.4 Sensitive analysis of the parameters in the long-term operation

3.4.1 Orthogonal test design

The sensible heat flux and the water vapor flux through the inner surface cause a direct impact on the heat and humidity load of the buildings (Wang et al., 2021b). The magnitude of these fluxes is affected by the indoor conditions (temperature and relative humidity of the indoor air) according to Eqs. (14) and (15). In addition, the operating temperature of the EDW has an obvious effect on the heat and moisture fluxes according to the above investigations. Therefore, an orthogonal test is performed to evaluate how much the discrepancies are induced by variations in these parameters.

In the published works, Barla et al. (2020) investigated the long-term thermal activation of the EDW at operating temperatures of approximately 26.5 °C in the heat injection season (summer) and 4 °C in the heat extraction season (winter). Xia et al. (2012) presented an experiment investigation of EDW at operating temperatures of 32, 35, and 38 °C. Additionally, Makasis et al. (2018) examines the suitability of energy diaphragm retaining walls for an underground train station based in the city of Melbourne, Australia, at the operating temperature between 0 and 40 °C. Therefore, in this section, several representative temperatures are chosen to represent how the EDW will operate. Moreover, based on the recommended indoor air conditioning parameters presented by Djongyang et al. (2010), the indoor relative humidity is set between 40% and 55%. The details are shown in Table 2. It should be noted that the indoor relative humidity (ϕ_indoor) is the same during the heat injection and heat extraction seasons. However, the temperatures of the heat exchanger and indoor air (T_indoor) change in a ramp trend in transition seasons. The trend is the same as that in Fig. 21. Besides, the temperature at the 30-day stable period is the average level of that in summer and winter.

To investigate the differences in outcomes resulting from the combination of these levels, 16 groups of cases are established according to the principle of orthogonal test design. Details of cases are given in Table 3.

3.4.2 Orthogonal test results and discussion

Both the discrepancies in the sensible heat flux and water vapor flux are compared. The results of Fig. 26(b) and (c) in Section 3.3 are selected as the benchmark. The relative discrepancies compared to the benchmark are calculated by Eq. (18):

$$\delta = \frac{\chi_{1-16} - \chi_{\text{benchmark}}}{\chi_{\text{benchmark}}} \times 100\%, \tag{18}$$

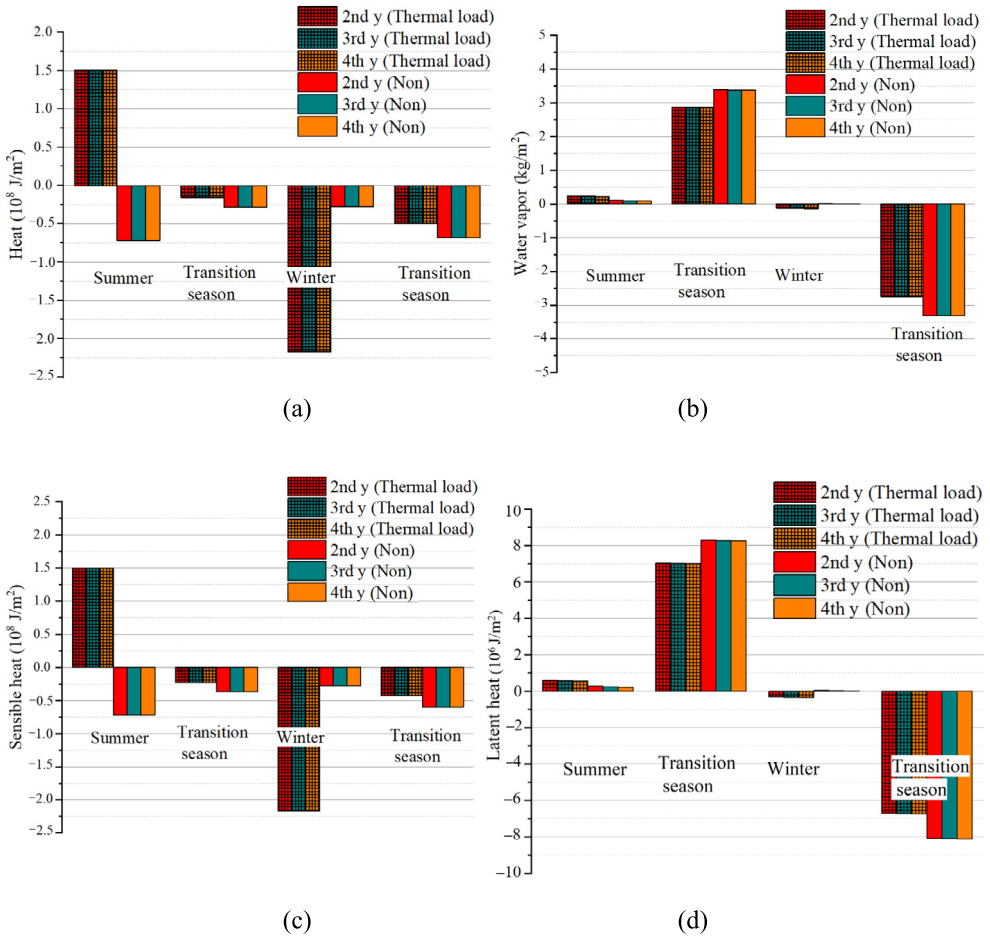

Fig. 26. Amount of the heat and moisture transfer in the seasons. (a) Total heat, (b) water vapor, (c) sensible heat, and (d) latent heat.

Table 2
Levels of the parameters.

Levels	T Heat exchanger (Summer)	T_indoor (Summer)	T Heat exchanger (Winter)	ϕ_indoor	T_indoor (Winter)
	S1	S2	S3	S4	S5
L1	31 °C	24 °C	3 °C	0.40	14 °C
L2	33 °C	25 °C	5 °C	0.45	16 °C
L3	35 °C	26 °C	7 °C	0.50	18 °C
L4	37 °C	27 °C	9 °C	0.55	20 °C

where the δ denotes the relative discrepancies between the cases and the benchmark; χ_{1-16} denotes the results of each case designed; $\chi_{benchmark}$ is the results in Section 3.3.

The relative changes in sensible heat flux and water vapour flux are summarised and compared by seasons. Transition season 1 is the period of transition from heat injection to heat extraction, while transition season 2 is the period of transition from heat extraction to heat injection. Results are listed in Table 4.

The polar analysis can help to reveal the magnitude of the impact induced by the parameters (Chen et al., 2024). The results are summarized in Table 5. R denotes the extremely poor, the details of which are listed in Tables A1 and A2 in Appendix A. It can be seen that in different seasons, the magnitude of the influence caused by each parameter is not the same. This is because the coupled heat and moisture transfer is a complex process, which can be affected by the temperature gradient, humidity gradient, moisture storage capacity of the material, local partial pressure of saturated water vapor, etc. In summer, the operating temperature of EDW has the greatest influence on heat flux and water vapor flux. The levels of indoor relative humidity are the most obvious parameter affecting water vapor flux in all the seasons.

Table 3
Orthogonal test design.

No.	S1	S2	S3	S4	S5
1	31 °C (L1)	24 °C (L1)	3 °C (L1)	0.40 (L1)	14 °C (L1)
2	31 °C (L1)	25 °C (L2)	5 °C (L2)	0.45 (L2)	16 °C (L2)
3	31 °C (L1)	26 °C (L3)	7 °C (L3)	0.50 (L3)	18 °C (L3)
4	31 °C (L1)	27 °C (L4)	9 °C (L4)	0.55 (L4)	20 °C (L4)
5	33 °C (L2)	24 °C (L1)	5 °C (L2)	0.50 (L3)	20 °C (L4)
6	33 °C (L2)	25 °C (L2)	3 °C (L1)	0.55 (L4)	18 °C (L3)
7	33 °C (L2)	26 °C (L3)	9 °C (L4)	0.40 (L1)	16 °C (L2)
8	33 °C (L2)	27 °C (L4)	7 °C (L3)	0.45 (L2)	14 °C (L1)
9	35 °C (L3)	24 °C (L1)	7 °C (L3)	0.50 (L4)	16 °C (L2)
10	35 °C (L3)	25 °C (L2)	9 °C (L4)	0.50 (L3)	14 °C (L1)
11	35 °C (L3)	26 °C (L3)	3 °C (L1)	0.45 (L2)	20 °C (L4)
12	35 °C (L3)	27 °C (L4)	5 °C (L2)	0.40 (L1)	8 °C (L3)
13	37 °C (L4)	24 °C (L1)	9 °C (L4)	0.45 (L2)	8 °C (L3)
14	37 °C (L4)	25 °C (L2)	7 °C (L3)	0.40 (L1)	20 °C (L4)
15	37 °C (L4)	26 °C (L3)	5 °C (L2)	0.55 (L4)	14 °C (L1)
16	37 °C (L4)	27 °C (L4)	3 °C (L1)	0.50 (L3)	16 °C (L2)

Table 4
Results of the relative changes between the cases and the benchmark.

No.	Heat flux variations (%)				Water vapor flux variations (%)			
	Summer	Transition season 1	Winter	Transition season 2	Summer	Transition season 1	Winter	Transition season 2
1	−22.44	0.57	−15.93	−1.02	−2.68	−48.94	−121.65	−32.56
2	−33.44	29.67	−15.70	21.94	−9.33	−35.65	−103.44	−25.33
3	−44.47	58.88	−15.47	45.07	−17.36	−21.22	−77.96	−17.49
4	−55.54	88.19	−15.26	68.33	−26.66	−5.18	−10.59	−9.77
5	0.03	57.84	15.55	44.97	−4.70	−1.86	68.88	−1.94
6	−10.95	84.56	15.68	70.09	−11.29	34.41	271.66	15.47
7	−22.47	−110.15	−46.63	−93.52	1.38	−59.25	−139.58	−41.86
8	−33.47	−83.52	−46.53	−69.17	−5.56	−40.41	−112.04	−31.23
9	22.22	−168.24	−31.02	−139.11	4.79	−23.17	−51.94	−17.67
10	11.11	−252.20	−61.80	−207.65	2.46	−36.69	−82.67	−28.58
11	−0.15	112.57	30.86	91.97	3.72	−5.45	−2.25	2.91
12	−11.41	28.28	−0.49	22.18	6.63	−36.53	−136.13	−19.99
13	44.17	−223.53	−31.17	−185.83	15.85	−40.72	−88.24	−26.65
14	32.90	−83.38	−0.50	−71.03	15.77	−42.11	−138.29	−23.21
15	22.36	−170.92	−30.89	−137.01	8.50	9.51	13.17	4.52
16	11.08	−30.26	−0.05	−21.60	7.79	11.52	27.55	8.82

Table 5
Polar analysis results.

	Heat flux	Water vapor flux
Summer	*R*: S1 > S2 > S4 > S3 > S5	*R*: S1 > S4 > S2 > S5 > S3
Transition season 1	*R*: S1 > S5 > S3 > S2 > S4	*R*: S4 > S3 > S5 > S1 > S2
Winter	*R*: S5 > S3 > S4 > S1 > S2	*R*: S4 > S3 > S1 > S5 > S2
Transition season 2	*R*: S3 > S1 > S5 > S2 > S4	*R*: S4 > S3 > S5 > S2 > S1

4 Conclusions

This paper proposes an approach for investigating the coupled heat and mass transfer process in the EDW based on the FDM. The algorithm is achieved with the programming language in MATLAB software. The behavior of the coupled heat and mass transfer process in the envelopes is investigated. The heat and moisture flux through the inner surface is focused.

The key conclusions are listed as follows:

(1) The moisture transfer process causes little impact on the temperature field of the surroundings and surface, but it will induce additional heat flux at the surface. If moisture transfer is not taken into account, the heat flux is underestimated by more than 3.43% in the case of heat extraction and by more than 3.90% in the case of heat injection.

(2) The sensible heat flux through the surface is over ten times greater than the latent heat flux, which is approximately 18.7 and −27.4 W/m^2 in summer and winter, respectively. Moreover, the peak latent heat flux to the conventional wall is reduced by 14.7% compared to the EDW, and the sensible heat flux is significantly increased by the operation of the EDW.
(3) The moisture flux is very significant in the transitional seasons, while it is minimal in summer and winter. The variation in the partial pressure of saturated water vapor and relative humidity at the inner surface is the primary cause. This transition season's effect-induced great moisture transfer may need to be considered when assessing the indoor humidity load. Ignoring this part may cause certain discrepancies.
(4) The moisture flux through the inner surface can be considered fully compensated in seasonal cycles. This indicates that the wet component in the surrounding soil causes little impact on the heat and moisture flux. The interaction between the inner surface and the indoor environment is relatively significant and should be taken seriously.
(5) In different seasons, the magnitude of the influence caused by the input parameters is irregular. In general, the operating temperature of the EDW has the greatest influence on the heat and water vapor fluxes in summer. Indoor relative humidity is the most obvious parameter affecting water vapor flux in all seasons.

Summarily, the coupled heat and moisture transfer in the EDW operation period will cause a nonnegligible impact on the hygrothermal load. This paper attempts to attract people's attention to the heat and moisture flux through the wall surface when applying EDW in underground constructions. However, only the coupled heat and moisture transfer process and their effect on the surface flux during an example long-running operation period of the EDW are investigated. More efforts are expected to analyze the behavior of the coupled heat and moisture transfer under varied periodic thermal load modes in further works.

Data availability

The data that support the findings of this study are available from the corresponding author upon reasonable request.

CRediT authorship contribution statement

Xu Zhou: Writing – original draft, Methodology, Investigation, Formal analysis, Data curation, Conceptualization. **Xiaoling Cao:** Supervision, Methodology, Funding acquisition, Conceptualization. **Ziyu Leng:** Writing – review & editing, Visualization, Validation, Software. **Chao Zeng:** Writing – review & editing, Validation, Software. **Yanping Yuan:** Supervision, Methodology, Funding acquisition, Conceptualization. **Shady Attia:** Writing – review & editing, Methodology.

Declaration of competing interest

The authors declare that they have no known competing financial interests or personal relationships that could have appeared to influence the work reported in this paper.

Acknowledgement

This work was supported by Sichuan Science and Technology Program (Grant No. 2021YFG0120).

Appendix A

A.1 Discreteness of control equation

The temperature can affect the moisture transfer process, meanwhile, the moisture content influences the magnitude of the heat transfer process. Therefore, in this study, the field of heat and moisture are computed together at every single time step.

Taking the heat transfer as an example, Eq. (11) can be expressed in the following form of Eq. (A1):

$$\begin{cases} A\frac{\partial T}{\partial t} = \nabla\left[A_\phi \nabla\phi + A_T \nabla T\right] \\ A = \rho_m c_m + w c_l \end{cases}. \tag{A1}$$

An integration step is performed within the control volume. Then, the governing equations of the coupled heat and moisture transfer can be described as a matrix form by adopting the central difference method at the discrete nodes:

$$\begin{bmatrix} -\frac{A_T}{\Delta x} & 2\frac{A_T}{\Delta x}+\frac{A}{\Delta t}\Delta x & -\frac{A_T}{\Delta x}-\frac{A_\phi}{\Delta x} & 2\frac{A_\phi}{\Delta x} & -\frac{A_\phi}{\Delta x} \\ -\frac{D_T}{\Delta x} & 2\frac{D_T}{\Delta x} & -\frac{D_T}{\Delta x}-\frac{D_\phi}{\Delta x} & 2\frac{D_\phi}{\Delta x}+\frac{\xi}{\Delta t}\Delta x & -\frac{D_\phi}{\Delta x} \end{bmatrix} \begin{bmatrix} T_{i-1}^1 \\ T_i^1 \\ T_{i+1}^1 \\ \phi_{i-1}^1 \\ \phi_i^1 \\ \phi_{i+1}^1 \end{bmatrix} = \begin{bmatrix} \frac{A}{\Delta t}\Delta x T_i^0 \\ \frac{\xi}{\Delta t}\Delta x \phi_i^0 \end{bmatrix}, \tag{A2}$$

where the superscript 1 denotes the state to be solved in the current time step; 0 represents the state already been solved in the previous time step.

For the two nodes adjacent to the heat exchanger. Combining with Fig. 4, the energy equation is converted into Eq. (A3), by substituting Eq. (17) into Eq. (A1):

$$A\frac{\partial T}{\partial t}\Delta x = A_\phi \nabla\phi + A_T \nabla T + A_T \frac{\left(T_f - T^1_{i(i+1)}\right)}{\frac{\Delta x}{2}}. \tag{A3}$$

Then the matrix for solving the nodes adjacent to the heat exchanger can be converted into the following form:

$$\begin{bmatrix} -\frac{A_T}{\Delta x} & 2\frac{A_T}{\Delta x}+2\frac{A_T}{\Delta x}+\frac{A}{\Delta t}\Delta x & -\frac{A_T}{\Delta x} & -\frac{A_\phi}{\Delta x} & 2\frac{A_\phi}{\Delta x} & -\frac{A_\phi}{\Delta x} \\ -\frac{D_T}{\Delta x} & 2\frac{D_T}{\Delta x} & -\frac{D_T}{\Delta x} & -\frac{D_\phi}{\Delta x} & 2\frac{D_\phi}{\Delta x}+\frac{\xi}{\Delta t}\Delta x & -\frac{D_\phi}{\Delta x} \end{bmatrix} \begin{bmatrix} T^1_{i-1} \\ T^1_i \\ T^1_{i+1} \\ \phi^1_{i-1} \\ \phi^1_i \\ \phi^1_{i+1} \end{bmatrix} = \begin{bmatrix} \frac{A}{\Delta t}\Delta x T^0_i + 2\frac{A_T}{\Delta x}T_f \\ \frac{\xi}{\Delta t}\Delta x \phi^0_i \end{bmatrix}. \tag{A4}$$

The EDW system consists of four main layers: mortar, EPS, concrete, and soil. An accurate result can be obtained by placing a node at the interface between the layers, as depicted in Fig. A1. The contact resistance of the thermal and moisture between different materials is ignored, and the heat and moisture capacity controlled by the "placed-node" can be described by Eqs. (A5) and (A6):

$$\begin{aligned} \rho_i c_i &= \frac{\frac{\Delta x_A}{2}(\rho_{i-1}c_{i-1}) + \frac{\Delta x_B}{2}(\rho_{i+1}c_{i+1})}{\frac{\Delta x_A}{2}+\frac{\Delta x_B}{2}} \\ &= \frac{\Delta x_A(\rho_{i-1}c_{i-1}) + \Delta x_B(\rho_{i+1}c_{i+1})}{\Delta x_A + \Delta x_B}, \end{aligned} \tag{A5}$$

$$\begin{cases} w_i = \frac{\frac{\Delta x_A}{2}w_{i-1}+\frac{\Delta x_B}{2}w_{i+1}}{\frac{\Delta x_A}{2}+\frac{\Delta x_B}{2}} \\ \xi_i = \frac{\partial w_i}{\partial \phi_i} = \frac{\frac{\Delta x_A}{2}\frac{\partial w_{i-1}}{\partial \phi_{i-1}}+\frac{\Delta x_B}{2}\frac{\partial w_{i+1}}{\partial \phi_{i+1}}}{\frac{\Delta x_A}{2}+\frac{\Delta x_B}{2}} = \frac{\Delta x_A \xi_{i-1}+\Delta x_B \xi_{i+1}}{\Delta x_A+\Delta x_B} \end{cases}. \tag{A6}$$

The discrete equations can also be expressed in the form of Eqs. (A7) and (A8) for the moisture content and temperature are continuous driving potentials.

$$\begin{aligned} &\frac{\Delta x_A(\rho_{i-1}c_{i-1}) + \Delta x_B(\rho_{i+1}c_{i+1})}{\Delta x_A + \Delta x_B}\cdot\frac{T^1_i - T^0_i}{\Delta t} = \\ &\frac{A_{T_{i+1}}\frac{(T^1_{i+1}-T^1_i)}{\Delta x_A} - A_{T_{i-1}}\frac{(T^1_i - T^1_{i-1})}{\Delta x_B}}{\Delta x} + \frac{A_{\phi_{i+1}}\frac{(\phi^1_{i+1}-\phi^1_i)}{\Delta x_A} - A_{\phi_{i-1}}\frac{(\phi^1_i-\phi^1_{i-1})}{\Delta x_B}}{\Delta x}, \end{aligned} \tag{A7}$$

$$\begin{aligned} &\frac{\Delta x_A \xi_{i-1} + \Delta x_B \xi_{i+1}}{\Delta x_A + \Delta x_B}\cdot\frac{\phi^1_i - \phi T^0_i}{\Delta t} = \\ &\frac{D_{T_{i+1}}\frac{(T^1_{i+1}-T^1_i)}{\Delta x_A} - D_{T_{i-1}}\frac{(T^1_i - T^1_{i-1})}{\Delta x_B}}{\Delta x} + \frac{D_{\phi_{i+1}}\frac{(\phi^1_{i+1}-\phi^1_i)}{\Delta x_A} - D_{\phi_{i-1}}\frac{(\phi^1_i-\phi^1_{i-1})}{\Delta x_B}}{\Delta x}. \end{aligned} \tag{A8}$$

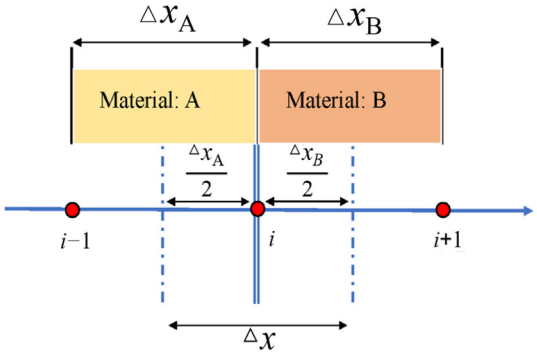

Fig. A1. Schematic of the coupled multilayer materials.

A.2 Polar analysis tables of the orthogonal test

K_1–K_4 represent the sum of the changes in the results of the five factors at the four levels. For example, these five numbers in the K_1 row of Table A1 are the sum of the heat flux changes (Table 4) corresponding to the parameters: temperature of heat exchanger in summer, indoor temperature in summer, temperature of heat exchanger in winter, indoor relative humidity, and indoor temperature in winter. k_1–k_4 are the K_1–K_4 divided by the number of levels (4 levels). "R" denotes the extremely poor of k_1 to k_4 in each parameter. For instance, the maximum and minimum k in summer in Table A1 to the parameter S1 are 27.63 and −38.97, and the extremely poor is 66.60.

Table A1
Polar analysis results of the influence on the heat flux.

Summer		S1	S2	S3	S4	S5
	K_1	−155.88	43.99	−22.46	−23.41	−22.44
	K_2	−66.86	−0.37	−22.45	−22.88	−22.62
	K_3	21.77	−44.74	−22.82	−22.24	−22.65
	K_4	110.51	−89.33	−22.72	−21.91	−22.75
	k_1	−38.97	11.00	−5.62	−5.85	−5.61
	k_2	−16.71	−0.09	−5.61	−5.72	−5.65
	k_3	5.44	−11.19	−5.70	−5.56	−5.66
	k_4	27.63	−22.33	−5.68	−5.48	−5.69
	R	**66.60**	**33.33**	**0.09**	**0.38**	**0.08**
Sorting	R: S1 > S2 > S4 > S3 > S5					
Transition season 1		S1	S2	S3	S4	S5
	K_1	177.31	−333.37	167.44	−164.69	−506.07
	K_2	−51.27	−221.34	−55.13	−164.81	−278.98
	K_3	−279.59	−109.62	−276.25	−165.74	−51.81
	K_4	−508.09	2.69	−497.70	−166.41	175.22
	k_1	44.33	−83.34	41.86	−41.17	−126.52
	k_2	−12.82	−55.34	−13.78	−41.2	−69.74
	k_3	−69.90	−27.40	−69.06	−41.43	−12.95
	k_4	−127.02	0.67	−124.42	−41.60	43.80
	R	171.35	84.01	166.28	0.42	170.32
Sorting	R: S1 > S5 > S3 > S2 > S4					
Winter		S1	S2	S3	S4	S5
	K_1	−62.35	−62.56	30.57	−63.55	−155.16
	K_2	−61.93	−62.33	−31.53	−62.54	−93.40
	K_3	−62.44	−62.13	−93.52	−61.76	−31.44
	K_4	−62.62	−62.32	−154.87	−61.49	30.66
	k_1	−15.59	−15.64	7.64	−15.89	−38.79
	k_2	−15.48	−15.58	−7.88	−15.63	−23.35
	k_3	−15.61	−15.53	−23.38	−15.44	−7.86
	k_4	−15.65	−15.58	−38.72	−15.37	7.67
	R	0.17	0.11	46.36	0.52	46.45
Sorting	R: S5 > S3 > S4 > S1 > S2					
Transition season 2		S1	S2	S3	S4	S5
	K_1	134.32	−280.99	139.44	−143.40	−414.86
	K_2	−47.63	−186.64	−47.92	−141.09	−232.28
	K_3	−232.61	−93.49	−234.24	−139.20	−48.49
	K_4	−415.46	−0.26	−418.67	−137.70	134.25
	k_1	33.58	−70.25	34.86	−35.85	−103.72
	k_2	−11.91	−46.66	−11.98	−35.27	−58.07
	k_3	−58.15	−23.37	−58.56	−34.80	−12.12
	k_4	−103.87	−0.06	−104.67	−34.42	33.56
	R	137.45	70.18	139.53	1.42	137.28
Sorting	R: S3 > S1 > S5 > S2 > S4					

Table A2
Polar analysis results of the influence on water vapor flux.

Summer		S1	S2	S3	S4	S5
	K_1	−56.03	13.26	−2.45	21.09	2.72
	K_2	−20.17	−2.38	1.10	4.68	4.63
	K_3	17.60	−3.77	−2.37	−11.80	−6.17
	K_4	47.91	−17.81	−6.97	−24.66	−11.87
	k_1	−14.01	3.31	−0.61	5.27	0.68
	k_2	−5.04	−0.60	0.28	1.17	1.16
	k_3	4.40	−0.94	−0.59	−2.95	−1.54
	k_4	11.98	−4.45	−1.74	−6.17	−2.97
	R	25.99	7.77	2.02	11.44	4.13
Sorting	R: S1 > S4 > S2 > S5 > S3					
Transition season 1		S1	S2	S3	S4	S5
	K_1	−111.00	−114.68	−8.46	−186.83	−116.52
	K_2	−67.11	−80.03	−64.52	−122.23	−106.55
	K_3	−101.84	−76.42	−126.91	−48.24	−64.06
	K_4	−61.79	−70.60	−141.84	15.56	−54.60
	k_1	−27.75	−28.67	−2.11	−46.71	−29.13
	k_2	−16.78	−20.01	−16.13	−30.56	−26.64
	k_3	−25.46	−19.10	−31.73	−12.06	−16.02
	k_4	−15.45	−17.65	−35.46	3.89	−13.65
	R	12.30	11.02	33.35	50.60	15.48
Sorting	R: S4 > S3 > S5 > S1 > S2					
Winter		S1	S2	S3	S4	S5
	K_1	−313.63	−192.95	175.31	−535.66	−303.20
	K_2	88.91	−52.75	−157.53	−305.97	−267.40
	K_3	−273.00	−206.62	−380.23	−64.20	−30.67
	K_4	−185.81	−231.21	−321.08	222.29	−82.26
	k_1	−78.41	−48.24	43.83	−133.91	−75.80
	k_2	22.23	−13.19	−39.38	−76.49	−66.85
	k_3	−68.25	−51.66	−95.06	−16.05	−7.67
	k_4	−46.45	−57.80	−80.27	55.57	−20.57
	R	100.64	44.62	138.89	189.49	68.13
Sorting	R: S4 > S3 > S1 > S5 > S2					
Transition season 2		S1	S2	S3	S4	S5
	K_1	−85.16	−78.82	−5.36	−117.63	−87.85
	K_2	−59.56	−61.65	−42.73	−80.31	−76.04
	K_3	−63.33	−51.92	−89.61	−39.19	−48.65
	K_4	−36.52	−52.17	−106.87	−7.45	−32.02
	k_1	−21.29	−19.71	−1.34	−29.41	−21.96
	k_2	−14.89	−15.41	−10.68	−20.08	−19.01
	k_3	−15.83	−12.98	−22.40	−9.80	−12.16
	k_4	−9.13	−13.04	−26.72	−1.86	−8.01
	R	12.16	6.73	25.38	27.54	13.96
Sorting	R: S4 > S3 > S5 > S2 > S1					

References

Adam, D., & Markiewicz, R. (2009). Energy from earth-coupled structures, foundations, tunnels and sewers. *Géotechnique*, 59(3), 229–236.

Barla, M., Di Donna, A., & Santi, A. (2020). Energy and mechanical aspects on the thermal activation of diaphragm walls for heating and cooling. *Renewable Energy*, 147, 2654–2663.

Bourne-Webb, P. J., Bodas Freitas, T. M., & da Costa Gonçalves, R. A. (2016). Thermal and mechanical aspects of the response of embedded retaining walls used as shallow geothermal heat exchangers. *Energy and Buildings*, 125, 130–141.

Branco, F., Tadeu, A., & Simes, N. (2004). Heat conduction across double brick walls via BEM. *Building and Environment*, 39(1), 51–58.

Brandl, H. (2006). Energy foundations and other thermo-active ground structures. *Géotechnique*, 56(2), 81–122.

Brandl, H. (2013). Thermo-active Ground-Source Structures for Heating and Cooling. *Procedia Engineering*, 57, 9–18.

British Standard Institution. (2007). EN 15026: *Hygrothermal Performance of Building Components and Building Elements-Assessment of Moisture Transfer by Numerical Simulation.*

Cao, X. L., Yuan, Y. P., Sun, L. L., Lei, B., Yu, N. Y., & Yang, X. J. (2015). Restoration performance of vertical ground heat exchanger with various intermittent ratios. *Geothermics*, 54, 115–121.

Chen, C., Mao, R. Y., Huang, G. Q., Wu, H. W., & Zhang, Z. J. (2024). Optimizing horizontal manifold arrangement for ground source heat pump using orthogonal testing. *Applied Thermal Engineering*, 243, 122582.

Colinart, T., Lelievre, D., & Glouannec, P. (2016). Experimental and numerical analysis of the transient hygrothermal behavior of multi-layered hemp concrete wall. *Energy and Buildings*, 112, 1–11.

Dai, Q. W., & Li, Z. L. (2019). Long-term mechanical performance of geothermal diaphragm walls in stiff clay. *Tunnelling and Underground Space Technology*, 94, 103113.

Di Donna, A., Cecinato, F., Loveridge, F., & Barla, M. (2017). Energy performance of diaphragm walls used as heat exchangers. *Proceedings of the Institution of Civil Engineers - Geotechnical Engineering*, 170(3), 232–245.

Di Donna, A., Loveridge, F., Piemontese, M., & Barla, M. (2021). The role of ground conditions on the heat exchange potential of energy walls. *Geomechanics for Energy and the Environment*, 25, 100199.

Djongyang, N., Tchinda, R., & Njomo, D. (2010). Thermal comfort: A review paper. *Renewable and Sustainable Energy Reviews*, 14(9), 2626–2640.

Dong, S. S., Li, X. Z., Tang, A. M., Pereira, J. M., Nguyen, V. T., Che, P., & Xiong, Z. Y. (2019). Thermo-mechanical behavior of energy diaphragm wall: Physical and numerical modelling. *Applied Thermal Engineering*, 146, 243–251.

Fang, A., Chen, Y., & Wu, L. (2020). Transient simulation of coupled heat and moisture transfer through multi-layer walls exposed to future climate in the hot and humid southern China area. *Sustainable Cities and Society*, 52, 101812.

Guimarães, A. S., Delgado, J. M. P. Q., & de Freitas, V. P. (2015). Influence of Mortar Joints on the Moisture Transfer in Layered Materials. In *Defect and Diffusion Forum* (vol. 365, pp. 160–165). Trans Tech Publications, Ltd.

Habert, J., & Burlon, S. (2015). *Modelling Thermo-active Diaphragm Walls.* Paper presented at the Second EAGE Workshop on Geomechanics and Energy, cp-466-00022.

Kumaran, M. (1996). IEA annex final report, Vo1. 3. 14–132.

Laloui, L., Nuth, M., & Vulliet, L. (2006). Experimental and numerical investigations of the behaviour of a heat exchanger pile. *International Journal for Numerical and Analytical Methods in Geomechanics*, 30(8), 763–781.

Li, K. S., Zhang, X., Han, X., & Zhu, D. M. (2009). Experimental Research of Water Vapor Permeability through Building Materials. *Journal of Building Materials*, 12(3), 288–291 (in Chinese).

Li, S. Y., Xia, C. C., Zhu, J. L., & Cheng, X. H. (2020). Centrifugal Model Test Study on Thermal Stress of Energy Diaphragm Wal. *Chinese Journal of Underground Space and Engineering*, 16(04), 1012–1020 (in Chinese).

Liu, R., & Huang, Y. W. (2018). Heat and moisture transfer characteristics of multilayer walls. *Energy Procedia*, 152, 324–329.

Liu, X., Chen, Y., Ge, H., Fazio, P., & Chen, G. (2015a). Numerical investigation for thermal performance of exterior walls of residential buildings with moisture transfer in hot summer and cold winter zone of China. *Energy and Buildings*, 93, 259–268.

Liu, X., Chen, Y., Ge, H., Fazio, P., & Chen, G. (2015b). Numerical investigation for thermal performance of exterior walls of residential buildings with moisture transfer in hot summer and cold winter zone of China. *Energy and Buildings*, 93(apr.), 259–268.

Luikov, A. V. (1964). Heat and mass transfer in capillary-porous bodies. *Advances in Heat Transfer*, 1(1), 123–184.

Luikov, A. V. (1975). Systems of differential equations of heat and mass transfer in capillary-porous bodies (review). *International Journal of Heat and Mass Transfer*, 18(1), 1–14.

Luikov, A. V., Shashkov, A. G., Vasiliev, L. L., & Fraiman, Y. E. (1968). Thermal conductivity of porous systems. *International Journal of Heat & Mass Transfer*, 11(2), 117–140.

Makasis, N., & Narsilio, G. A. (2020). Energy diaphragm wall thermal design: The effects of pipe configuration and spacing. *Renewable Energy*, 154, 476–487.

Makasis, N., Narsilio, G. A., Bidarmaghz, A., & Johnston, I. W. (2018). The application of retaining walls and slabs as energy structures in underground train stations. *Energy Geotechnics*, 43–50.

Makasis, N., Narsilio, G. A., Bidarmaghz, A., Johnston, I. W., & Zhong, Y. (2020). The importance of boundary conditions on the modelling of energy retaining walls. *Computers and Geotechnics*, 120.

Moon, H. J., Ryu, S. H., & Kim, J. T. (2014). The effect of moisture transportation on energy efficiency and IAQ in residential buildings. *Energy and Buildings*, 75, 439–446.

Rui, Y., & Yin, M. (2018). Thermo-hydro-mechanical coupling analysis of a thermo-active diaphragm wall. *Canadian Geotechnical Journal*, 55(5), 720–735.

Sailer, E., Taborda, D. M. G., Zdravković, L., & Potts, D. M. (2019). Fundamentals of the coupled thermo-hydro-mechanical behaviour of thermo-active retaining walls. *Computers and Geotechnics*, 109, 189–203.

Steeman, H. J., Van Belleghem, M., Janssens, A., & De Paepe, M. (2009). Coupled simulation of heat and moisture transport in air and porous materials for the assessment of moisture related damage. *Building and Environment*, 44(10), 2176–2184.

Sterpi, D., Tomaselli, G., & Angelotti, A. (2020). Energy performance of ground heat exchangers embedded in diaphragm walls: Field observations and optimization by numerical modelling. *Renewable Energy*, 147, 2748–2760.

Wang, Y. Y., Fan, Y., Wang, D. J., Liu, Y. F., & Liu, J. P. (2021a). The effect of moisture transfer on the inner surface thermal performance and the thermal transmittance of the roof-wall corner building node in high-temperature and high-humidity areas. *Journal of Building Engineering*, 44.

Wang, Y. Y., Jiang, C., Liu, Y. F., Wang, D. J., & Liu, J. P. (2018). The effect of heat and moisture coupling migration of ground structure without damp-proof course on the indoor floor surface temperature and humidity: Experimental study. *Energy and Buildings*, 158, 580–594.

Wang, Y. Y., Tian, Y., Zhao, Z. J., Wang, D. J., Liu, Y. F., & Liu, J. P. (2021b). Effect of moisture transfer on heat transfer through exterior corners of cooled buildings in hot and humid areas. *Journal of Building Engineering*, 43.

Wang, Z. H., Wang, F. H., Ma, Z. J., Wang, X. K., & Wu, X. Z. (2016). Research of heat and moisture transfer influence on the characteristics of the ground heat pump exchangers in unsaturated soil. *Energy and Buildings*, 130, 140–149.

Xia, C. C., Sun, M., Zhang, G. Z., Xiao, S. G., & Zou, Y. C. (2012). Experimental study on geothermal heat exchangers buried in diaphragm walls. *Energy and Buildings*, 52, 50–55.

Xia, C. C., Zhu, J. L., & Cao, S. D. (2014). Research on Thermal Stress Induced by the Heat Exchanger Pipes Buried in the Diaphragm Wall. *Chinese Journal of Underground Space and Engineering*, 10(1), 90–95 (in Chinese).

Xu, C. C., Li, S. H., & Zou, K. K. (2019). Study of heat and moisture transfer in internal and external wall insulation configurations. *Journal of Building Engineering*, 24.

Ministry of Housing and Urban-Rural Development of the People's Republic of China. (2016). *GB* 50176—2016: *Code for thermal design of civil building*. (in Chinese).

Sterpi, D., Angelotti, A., Corti, D., & Ramus, M. (2014). *Numerical analysis of heat transfer in thermo-active diaphragm walls*. Paper presented at the *Proceedings of the* 8*th European Conference on Numerical Methods in Geotechnical Engineering*, 1043–1048.

Yan, Z. F. (2003). *Dynamic Modelling of the Indoor Thermal and Humidity Environment in the Adobe Buildings.* [Master's thesis, Xi'an University of Architecture and Technology]. (in Chinese).

Yuan, Y. P., Cao, X. L., Sun, L. L., Lei, B., & Yu, N. Y. (2012). Ground source heat pump system: A review of simulation in China. *Renewable and Sustainable Energy Reviews*, 16(9), 6814–6822.

Zanden, A. J. J. V. D., & Schoenmakers, A. M. E. (1996). The influence of sorption isotherms on the drying of porous materials. *International Journal of Heat and Mass Transfer*, 39(11), 2319–2327.

Zeng, C., Tang, F., Yuan, Y., Cao, X., Haghighat, F., & Panchabikesan, K. (2021). Thermal performance of energy diaphragm wall (EDW) adjacent to air-conditioned space from the underground-engineering perspective. *Geothermics*, 91.

Zhou, S. Z., Zhang, R. Y., & Zhang, C. (2002). *Climatology and Meteorology*. Beijing: High Education Press (in Chinese).